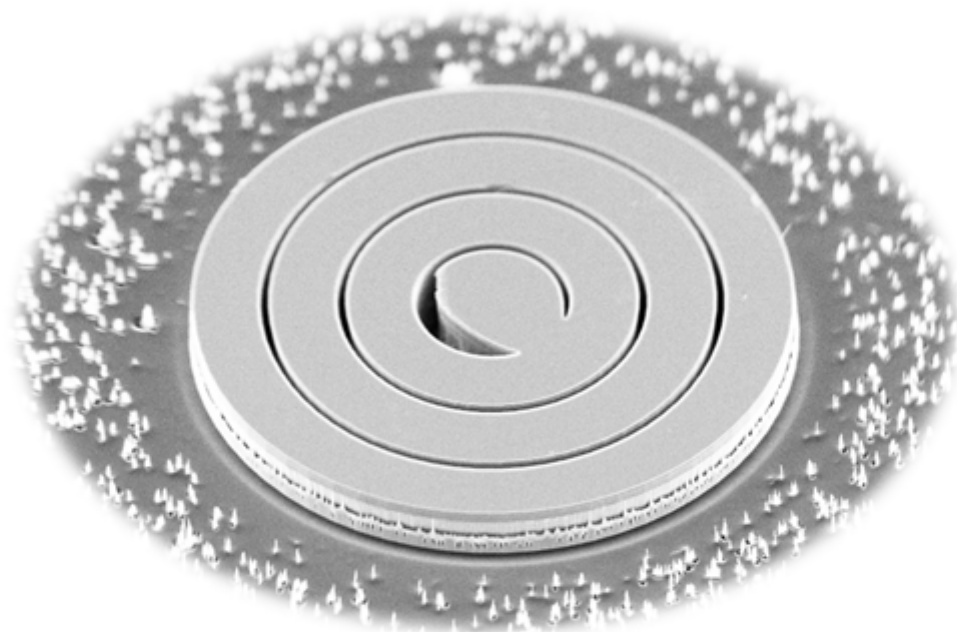


Master's Thesis

Fabrication of High Aspect Ratio Microstructures using Time Multiplexed Reactive Ion Etching

Anders Tang

Supervisor:
Esben Skovsen



Title:

Fabrication of High Aspect Ratio Microstructures using Time Multiplexed Reactive Ion Etching

Abstract:

The main objective of this Master's thesis has been to fabricate a gradient index lens, based on a theoretical design by Brincker and Karlsen [1]. The fabrication of the gradient index lens utilizes the deep reactive ion etching process called the Bosch process, in an attempt to create high aspect ratio microstructures.

A systematic optimization of the Bosch process, utilizing SF_6 as an etching gas and C_3F_8 as a passivation gas in a reactive ion etching system, was carried out. The Bosch process was optimized and structures with vertical sidewalls, and an aspect ratio of 22, was successfully fabricated. The Bosch process showed a high stability and good profile control.

Chromium was used as a hard mask and showed a high selectivity. Microtrenching was observed under certain structural conditions and resulted in a non-uniform etch rate.

The limiting factor of the aspect ratio was the thickness of the masking material. To achieve an aspect ratio higher than 22, further optimization of the process has to be carried out.

Project Period:

9-10. Semester, Spring 2015

Project Group:

5.240

Group Member:

Anders Tang

Supervisors:

Esben Skovsen

Special Thanks To:

Peter Kjær Kristensen
Deyong Wang

Number Printed: 3

Number of Pages: 69

Closing Date: 31-08-2015



Preface

This Master's thesis is written by group 5.230 which consists of a nanotechnology student at the 10th semester at Aalborg University. The thesis is a project running from September, 2014 to September, 2015.

Reading Guide

Throughout the report, references to different sources will be made; these will be found on the form [#] where the number in the square brackets refers to a specific source in the bibliography at the end of the report. In the bibliography the sources will be listed with its title, author, and other relevant information depending on whether the source is a book, article, or web page. If the bibliographic references are listed after a specific section it indicates that the reference applies to all of the above if nothing else is stated.

Tables and figures are numbered after the number of the chapter in which they are placed. Hence the first figure in chapter 4 would be named 'Figure 4.1' whereas the next one would be 'Figure 4.2' etc.. Since tables are numbered according to the same system, it is possible to find both 'Table 4.1' and 'Figure 4.1' in the same chapter. For each figure/table there is a short descriptive caption that will be made together with a bibliographic reference where necessary.

There is a CD attached to the back cover of the report. This CD includes an electronic version of the report, raw data and pictures.

Acknowledgements

First and foremost, I would like to thank my supervisor, Esben Skovsen for his guidance and advice, and his enthusiasm throughout the entire project.

In addition, a thank you to Peter Kjær Kristensen and Deyong Wang, who not only assisted me with some steps of the fabrication and characterization process, but also helped me to overcome all the hardships found during the experiments.

Aalborg University, September 2015

Anders Tang

Abbreviations

| | | |
|------|---|----------------------------------|
| APC | = | Automatic Pressure Control |
| AR | = | Aspect Ratio |
| ARDE | = | Aspect Ratio Dependant Etch |
| CVD | = | Chemical Vapour Deposition |
| DRIE | = | Deep Reactive Ion Etching |
| GRIN | = | Gradient Index |
| HAR | = | High Aspect Ratio |
| IAD | = | Ion Angular Distribution |
| ICP | = | Inductively Coupled Plasma |
| IR | = | Infrared |
| MEMS | = | Micro Electro-Mechanical Systems |
| PCA | = | Photoconductive Antenna |
| RIE | = | Reactive Ion Etch |
| SEM | = | Scanning Electron Microscope |
| SIL | = | Solid Immersion Lens |
| THz | = | TeraHertz |

Contents

- 1 Introduction** **1**
- 1.1 Different Ways to Etch 7
- 1.2 Reactive Ion Etching 10
- 1.3 Deep Reactive Ion Etching in Silicon 11
- 1.4 Process Parameters 13
- 1.5 Etch Mask 14
- 1.6 Passivation Step 15
- 1.7 Etch Rate 16
- 1.8 Profile Control 18
- 1.9 ARDE and RIE Lag 20
- 1.10 Micrograss 22
- 1.11 Resume 22
- 1.12 Project Goal 23

- 2 Experimental Procedure** **25**

- 3 Results and Discussion** **31**
- 3.1 Results 31
- 3.2 Discussion 54

- 4 Conclusion** **63**

- Bibliography** **65**

- A Appendix** **69**

Introduction 1

The THz regime is an interesting one, since THz radiation can pass through clothing, paper, wood, masonry, plastic, and ceramics, but not metals or water. THz radiation is the electromagnetic waves, at frequencies in the region of the electromagnetic spectrum, between 0.3 THz and 3 THz. This corresponds to the submillimeter wavelength range, between 1 mm (high-frequency edge of the microwave band) and 100 mm (long-wavelength edge of far-infrared light).

THz radiation is nonionizing, meaning the photons do not have enough energy to knock electrons of atoms, but it still stimulates the molecular and electronic motion in many material, it does so by being reflected off some, propagating through some, and being absorbed by the rest. This makes it ideal for different applications such as spectroscopy and non-invasive detection of cancer in humans. [2] [3]

The most common spectroscopy techniques, that can be compared to THz spectroscopy, are Raman and IR spectroscopy. All these techniques involves illuminating a sample with a laser beam and measuring the amount of scattered/absorbed light.

Raman and IR spectroscopy cannot detect as many resonant states as can THz spectroscopy, because THz photons are sensitive to the vibrational states of the entire molecule as opposed to just a bond or charge state as is the case with Raman and IR spectroscopy.

THz spectroscopy can be used in the discerning between single-stranded DNA and double-stranded (hybridized) DNA. This makes it crucial to a number of biological studies. THz spectroscopy can also be used to detect variation in the DNA sequence. This can help doctors determine whether or not the prescribed medicine will affect the individual person, by identifying the gene. [2]

THz radiation have an application within the security branch. Everyday materials are semi-transparent to THz radiation, and due to this it can be used to scan packages without opening them. This is useful if the package is suspected to contain explosives or other dangerous materials. The individual explosives exhibit individual spectra responses in the THz frequency range, see figure 1.1. This spectral response is called a "fingerprint" and it is different for individual explosives. The explosive RDX, which is a mixture of a number of military and commercial plastic explosives such as C4, PE4, and Semtex, has a very strong response at approximately 0.8 THz. Most other explosives have their lowest frequency responses nearer 2 THz. [3]

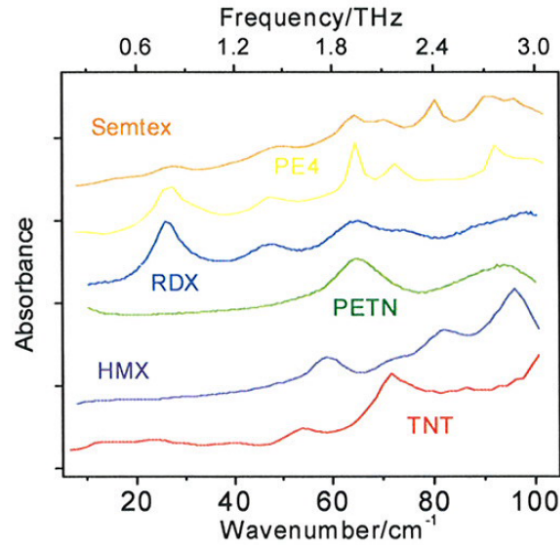


Figure 1.1: Absorption spectra of different explosives. [2]

Generation of THz Radiation

Generation of THz-pulses can be done by repeating a shorting of photo-conducting antennas using a femtosecond laser, but it can be hard to detect the THz signal from the photo-conducting antenna (PCA), often a lens is used to minimize the loss created by internal reflection. The internal reflection problem arises due to the material choice of the photo-conducting antenna, which is typically semi-insulating GaAs or high resistivity silicon. These materials have high refractive indexes that result in a very small critical angle. The lens used to couple the radiation to air can be designed to either collimate or focus the radiation, the lens is typically made from high resistivity silicon .

The substrate lens, of the design seen in figure 1.2, was first used by Exter et. al [4]. The design was used and investigated by Jepsen and Keiding [5]. They successfully showed that by using a truncated spherical silicon substrate lens, 21% of the power generated by the dipole can be detected. [2] [4] [5]

The truncated spherical lens structure gives the antenna some bulkiness, which makes integrated components large and more difficult to produce. The lens is expensive and is often bought separate to the antenna, which makes it even more expensive. Also in order for the lens effectiveness to be high it is important that the lens is aligned correctly relative to the gap of the photo conductive antenna, see figure 1.2. A small misalignment in the order of microns, will result in a distortion of the radiation.

An integrated lens design was proposed by Brincker and Karlsen, [1]. It is a gradient index (GRIN) lens design, that is fabricated into the antenna. This should make for a more compact and simpler to use PCA with integrated lens, than the PCA with a mounted lens. Their theoretical results show that with an aspect ratio (AR) of 40, 20% of the generated power would be effectively transmitted.

1.0.1 GRIN Lens

A GRIN lens is a lens that has a gradually varying refractive index (n) throughout the material. This inhomogeneous lens changes the way light propagates through it, the wave front slows down in the

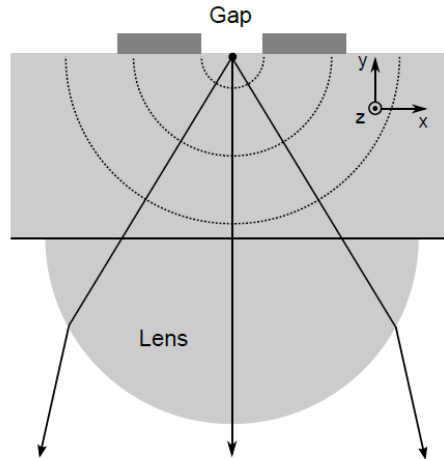


Figure 1.2: This figure show the basic concept behind the substrate lens. [1]

optically dense regions and speed up in the less dense regions, this can promote bending of the wave front. By utilizing this a lens with a flat surface can be created. A variety of these flat lenses are commercially available. The applications for this type of lens is vast and can be found in things such as laser printers, optical fibres, and other things. [6]

There are different ways to design a GRIN lens. Brincker and Karlsen, 2014 [1] designed a lens structure that utilizes the fact that a refractive index in a material can be changed by etching trenches in a material that is repeated with a period. This works as long as the period is much smaller than the wavelength of the incoming radiation. The wave will then not see the individual material-air interfaces but behave as if propagating through a material with an effective dielectric constant ϵ_{eff} , remember that $\epsilon_{eff}=n_{eff}^2$. By varying the refractive index in the plane parallel to the surface of the substrate, it is possible to get a lens that acts as a focusing lens. The basic concept of the lens can be seen in figure 1.3. [1]

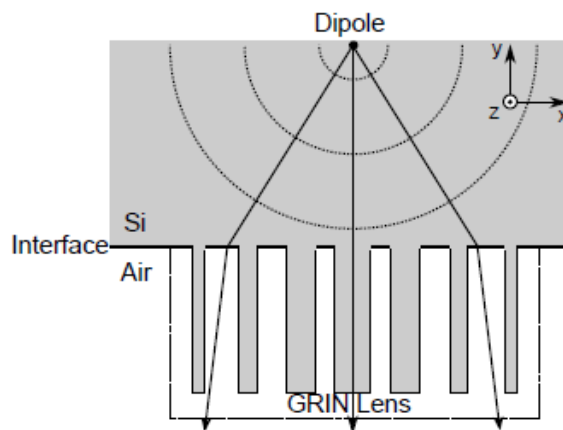


Figure 1.3: The basic concept for the GRIN lens, it shows how the lens design, created by Brincker and Karlsen [1], is integrated onto the PCA and how it works in principle. The dipole is the THz generator. [1]

1.0.2 Other GRIN Lens Designs

The creation of other GRIN lens designs for THz radiation are investigated by researchers all over the world. This section will briefly discuss three different lens designs and the advantages and disadvantages of these designs compared to the design suggested by Brincker and Karlsen, 2014 [1]

The first design by Saha et al., 2013 [7] is a multilevel diffractive lens. They fabricated 4-level and 16-level lens designs and investigated the properties of the lenses. The design will be referred to as design 1. The second design by Park et al., 2014 [8] is a GRIN lens design working on the same basic principle as the design suggested by Brincker and Karlsen, 2014 [1], where instead of etching grooves in a silicon wafer, the etching is through the entirety of the wafer. This design will be referred to as design 2.

The third lens design by Savini, et al., 2012 [9] is also a GRIN lens, it utilizes the fact that a change in refractive index can be achieved by creating a metal grid on top of the silicon wafer. This design will be referred to as design 3.

The main difference between these designs are their efficiency, bandwidth, size of the lens, and the complexity of the fabrication procedure. These differences will be discussed and compared to the theoretical design by Brincker and Karlsen [1].

Design 1 is fabricated in two different versions, the 4-level and the 16-level version. A sketch and a SEM picture of the 16-level version can be seen in figure 1.4. The difference between the 4- and 16-level designs are the complexity of fabricating the lens structure, where the 4-level lens is the less complicated. This increase in complexity has some advantages, the 16-level lens couples around 90% of the radiation to air, where as the 4-level lens only couples 40%. Design 1 is optimized to a single frequency, namely the frequency that is used to characterize the lenses, which is 2.52 THz. The beam profile for the 16-level lens is much sharper and the spot size is smaller compared to the 4-level design. Both the 4-level and the 16-level lens is 45 mm in diameter.

Design 1 is very efficient in the coupling of THz radiation however the monochromatic nature of the lens is a disadvantage for many applications.

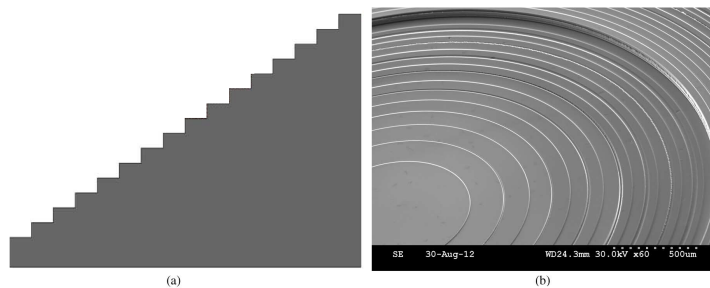


Figure 1.4: This figure show two pictures. (Left) A sketch of the 16-level design, (Right) A SEM picture of the 16-level design take at an angle of 60°. [7]

Design 2 is a GRIN lens fabricated by etching holes through the Si substrate in a hexagonal lattice, figure 1.5 show a picture of the lens. The refractive index is varied by changing the fillfactor¹ and the period of the unit cell. The Si through-hole arrays were fabricated using photolithography and deep reactive ion etching (DRIE). Two types of GRIN lenses were designed, a focusing lens and a solid immersion lens (SIL). The stacked lens design, involving the two types of lenses, show a high performance. The diameter

¹The ratio between the amount of Si and the amount of air in the unit cell.

of the lenses are 4 mm. The intensity of the radiation compared to a setup without a lens, has a peak enhancement of 10.3 times at 0.26 THz and an average enhancement of 4.2 times at 0.1–1 THz. The operating bandwidth of this lens is 1.2 THz.

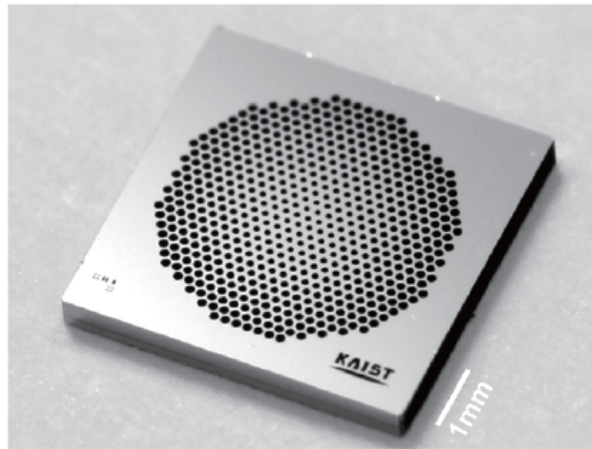


Figure 1.5: This shows a photographic image of the Si-GRIN lens (lens diameter: 4 mm). It can be seen that the spacing between the holes vary with respect to the radius. [8]

Design 3 is a GRIN lens fabricated by creating a metal grid to create a varying refractive index. The GRIN lens was created using 100 μ m thick polypropylene layers to separate the metal grids and create a robust lens. The lens consists of 200 layers of polypropylene, which makes the thickness 2mm. The lens is 10cm in diameter. The efficiency of the GRIN lens was compare to a HDPE lens² setup. The relative efficiency of the GRIN lens in the 0.1-0.35 THz regime is around 55%, but then it drops drastically, at 0.5 THz it is below 20%. Above 0.5 THz the efficiency quickly drops below 10%. The bandwidth of the GRIN lens is the most effective regime and is from 0.1 to 0.35 THz.

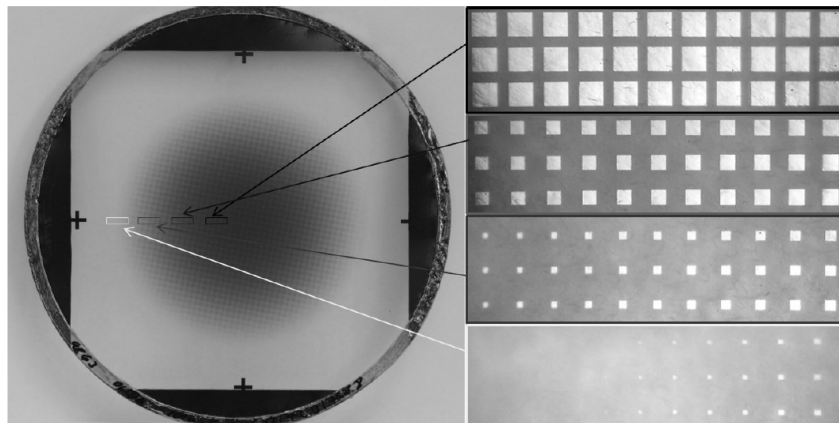


Figure 1.6: The figure (left) shows the GRIN lens and (right) that the metal grid changes with respect to distance. [9]

²High Density Polyethylene lens special designed for THz radiation, 7 cm in diameter and focal length = 175mm

The design proposed by Brincker and Karlsen, 2014 [1] is a GRIN lens created by etching trenches of air that is repeat with a period into a substrate, a sketch of the design as seen form above can be seen in figure 1.7. This design will be refereed to as design 4 in this section.

The theoretical GRIN lens is $700\ \mu\text{m}$ in diameter and $100\ \mu\text{m}$ thick, the thickness is the thickness of the lens not of the substrate which it is integrated into. The lens effectively transmits 20% of the radiation at 1 THz. The results also show that the only theoretical limitations of the lens is caused by the limitations created by the PCA. The limitation of the PCA is created during the THz generation, a pulsed laser that produces pulses of approximately $100\ \text{fs}$ is used and the generation does not typically exceed 4-5 THz. The bandwidth of the GRIN lens would then range from 0.1–5 THz approximately.

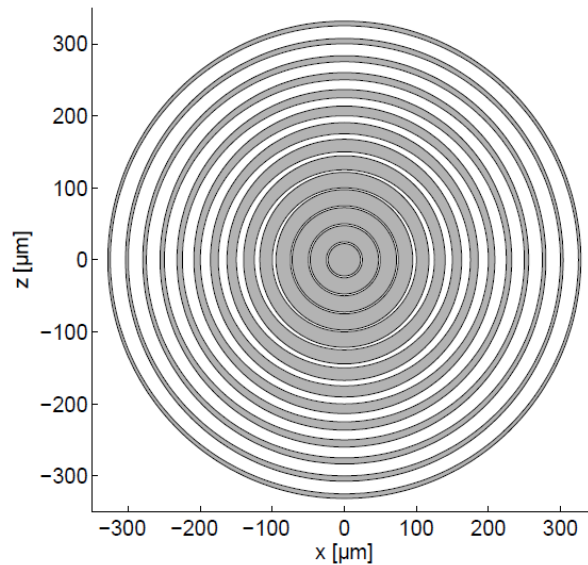


Figure 1.7: The figure shows a sketch of the GRIN lens design from above. [1]

The entire idea behind this project revolves around a small lens design, this design need to have a broad bandwidth and have the ability to be implemented onto the PCA. Design 1 has the possibility to be implemented onto the PCA since it is etched into Si just like design 4. The same would work for design 2 with some alterations, since if the substrate is etched through, the entire idea of having it integrated as part of the PCA is ruined since this would destroy the PCA. The alteration could be to etch deep holes in the PCA, this would however require a thick PCA. Design 3 also has the possibility to be integrated into the PCA since the metal mesh layer could simply be fabricated on top of the PCA. So basically all of the designs investigated as alternatives to design 4, can be implemented as part of the PCA.

The required bandwidth is dependant on the application. A broad bandwidth is preferable, since it leads to a wider range of applications. The application for detection of explosives through packaging is based on the principle that all explosives have individual detectable "THz fingerprints". This detection of "fingerprints" require a broadband signal and in the designs investigated, the lens is the limiting factor. A broad bandwidth is required since the "fingerprint" of e.g. PETN is best detected in the 0.3–3 THz range. If the design is to be used for detection of explosives then only design 4 can be used. Since it is the only design with the required bandwidth.

THz spectroscopy used for lab work is also an interesting application. THz spectroscopy can be used to

investigate everything from solids to gases. The THz spectroscopy can even be used for the comparison of DNA in the 0.1–1 THz range.

These two examples clearly show that all of the designs with a broad bandwidth have an application. According to Rostami et al. [2] the most used frequencies are ranging from 0.3–3 THz. All of the designs have different applications but design 4 can be used for a wider array of applications due to the bandwidth. [2] [3]

Efficiency is also an important factor. If the efficiency is small compared to that of the normal hemispherical lens, the lens with the lower efficiency need to have other trademarks to counter the lower efficiency. This is where some of the other designs have the ability to be implemented directly onto the PCA, which can reduce the misalignment loss and the reduced cost since the PCA + lens comes as a complete package.

The size of the designs also have some importance. The lens size is very dependent on the application. The design investigated previously in this section have sizes that range from 10 cm to only 700 μm . The implementation of the lens design directly onto the PCA reduces the overall size and complexity of the component. This will further enhance the components implementation in portable applications such as portable bomb detection. [3]

All of the designs investigated have their pros and cons, but design 4 have a superior broadband and size that far exceeds the other designs. Design 4 is still only theoretical and needs to be fabricated before any real comparison can be made. The fabrication and characterization of this design is the main goal of this project.

1.1 Different Ways to Etch

The main goal is to fabricate a GRIN lens based on the design suggested by Brincker and Karlsen, 2014 [1]. Different etching techniques need to be investigated, to best choose the right procedure to create this microstructure. The various etching techniques can be divided into wet and dry etching. In this section the different wet and dry etching techniques, will briefly be discussed. In the end of this section there will be a summary weighing the pros and cons of each technique, to find the best suitable.

The two important parameters for any etching process are selectivity and directionality. These two are the key parameters in determining if an etch is isotropic or anisotropic. Selectivity is the degree to which the etchant can differentiate between the masking layer and the layer to be etched. Directionality relates to the etch profile under the mask. An etch can either have isotropic or anisotropic nature. In an isotropic etch, the etchant attacks the material in all directions at the same rate, hence creating a semicircular profile under the mask. In an anisotropic etch, the etching is strongest in one direction, so the etchant attacks the material at different rates depending on the direction, thus creating a less semicircular profile. [10]

1.1.1 Wet Etch

In micro/nanofabrication wet etching is an important technique. A standard wet etching is almost isotropic and show a superior selectivity to the masking layer in comparison to dry etch. Silicon dioxide etching is normally done with buffered HF solution, and the most common masking materials are photoresist and silicon nitride. [10]

Not all wet etchings are isotropic. In the 1960's an anisotropic etch of silicon was achieved. This is considered to mark the beginning of micromachining. The three most important silicon etchants, used for anisotropic etching in silicon, are potassium hydroxide, ethylene diamine pyrocatechol, and tetramethyl ammonium hydroxide. These are all anisotropic etchants that etch silicon along preferred crystallographic directions. The etch rate (typically around $1 \mu\text{m}/\text{min}$) depends on the concentration and the temperature. The most used masking materials, for anisotropic wet etchings, are silicon dioxide and nitride, where nitride are best for long etch times. An example of anisotropic etch using potassium hydroxide can be seen in 1.8. Many studies have investigated the etch rates for the $\{111\}$, $\{100\}$, and $\{110\}$ planes, e.g. Bassous., 1978 [11]. When using the right chemical composition, the silicon etch rates at the $\{111\}$ surface is much slower than those on the $\{100\}$ and the $\{110\}$ planes. For example the etch rate on $\{110\}$ plane can be several hundred times the etch rate of the $\{111\}$ plane. Using the right chemical composition and a suitable mask, a rectangular groove with vertical side-walls and a high aspect ratio (HAR) can be fabricated on the $\{110\}$ plane. An AR as high as 400 can be achieved. [10] [12]

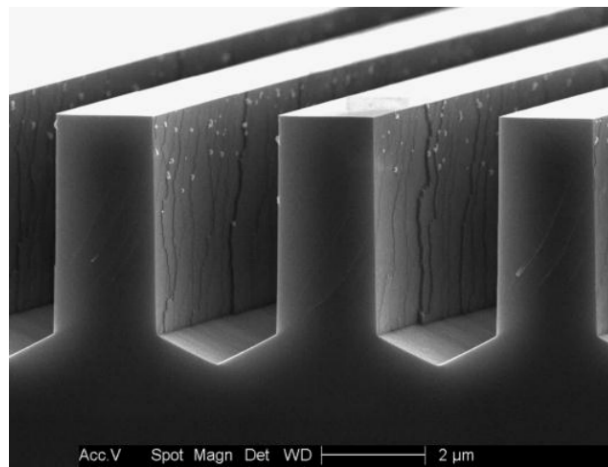


Figure 1.8: The figure shows a structure achieve by anisotropic potassium hydroxide based etching of Si. [13]

1.1.2 Dry Etch

Most dry etching techniques are plasma based. The three basic dry etching techniques are high-pressure plasma etching, reactive ion etching (RIE), and ion milling.

Ion milling is a technique that utilizes accelerated inert ions, e.g. Ar^+ . They strike the surface perpendicular and hereby remove material. Ion milling characteristics are very low etch rate (few nm/min) and poor selectivity. This process is mostly used to etch very thin layers of material. This technique operates at pressures around 10^{-4} - 10^{-3} Torr.

The high-pressure plasma etching technique operates at pressures around 0.1-5 Torr. This technique uses highly reactive species that react with the material to be etched. The product from the reaction between the material and the reactive species is volatile, so it diffuse away and new material is exposed. [10]

RIE, also called ion-assisted etching, is a combination of a physical and chemical process. In this technique the reactive species only react with the material when it is "activated" by the collision of incident ions from the plasma. The direction of the ion velocity produces more collisions in the horizontal surface than in the walls, this results in a faster etch rate in the vertical direction. To further increase the anisotropy, side wall passivation methods are used in some cases. [10]

Dry etching can also be performed in a non-plasma environment, if the etching gasses are reactive enough. This dry etching process can be carried out in a simple chamber with gas feeding and pumping capabilities. An example is HF vapour etching of silicon dioxide. This process is very isotropic and is typically used to etch of layers and release structures. [10]

1.1.3 Summary

The choice between wet etch and dry etch depends on a lot of factors, e.g what material is etched, how is the structure, are there different materials, how thick is the structure, and so on. Below is a summation with the general advantages regarding RIE and wet etching:

For RIE

- Some material can only be etched by plasma
- RIE process are simpler in some cases compared to wet etching
- The use of a photoresist, as making layer, is enough for many structures
- Etching is only one side, meaning no backside protection is needed
- High etch rate: 3-50 $\mu\text{m}/\text{min}$ for silicon vs. 1 $\mu\text{m}/\text{min}$ for KOH wet etching of silicon
- The profile can be controlled can be changed by changing the process parameters
- HAR structures can be made
- Not restricted by crystal planes

For wet etch

- Wet etching is simple
- Material that are hard to etch in RIE are some times easily etched in wet etch
- Wet etching is inexpensive compared to RIE
- Selectivity is often better in wet etch compared to RIE
- HAR structures can be made

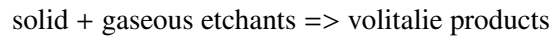
Some of the downsides to wet etching, such as large undercut, crystal plane dependant etching, and the increase in complexity of anisotropic etching, has in recent years pushed the etching of HAR and Micro Electro-Mechanical System (MEMS) structures towards dry etching. [10] [14]

The GRIN lens design by Brincker and Karlsen, [1] require a HAR structure and controllable profile angle. Therefore the fabrication of the lens will be carried out using dry etching. Since a HAR structure is needed it would seem that the RIE process combined with a passivation method is best suited. How to achieve HAR structures using dry etching will be further investigated in the coming sections.

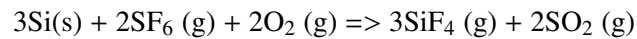
1.2 Reactive Ion Etching

This section will discuss the basic behind RIE chemistry and the RIE process. It will also briefly discuss the difference between RIE and DRIE reactors. This is done to have a better understanding regarding RIE to better understand the basic RIE mechanisms.

RIE is a combination of physical and chemical effects, it can be used to remove unwanted material. A wet etch process rely on the solubility of the etch products, the RIE process rely on the volatility. The reaction inside a RIE reactor can be simplified to:



An example of this is one of the most used silicon etchings, the etching of solid Si using gaseous SF₆ and O₂.



RIE is a plasma etching technique, where the plasma is created inside a chamber. Typically a plasma is initiated in the chamber by applying a strong RF electromagnetic field to the electrodes. The field is typically set to a frequency of 13.56 megahertz. If the voltage is high enough, typically between 100-1000 V, the oscillating electric field will ionizes the gas molecules by stripping them of electrons. This will create a large number of ions and free electrons. The electric field in the chamber will accelerate the electrons towards the positively charged anode and the ions will be accelerated towards the negatively charged cathodes. Due to the high frequency only the electrons responds to the instantaneous electric field and they oscillate back and forth within the positive ions space charge cloud. As the electrons oscillate back and forth they sometimes strike the electrodes and can be absorbed and this develops a large negative voltage at the electrodes. So the plasma is no longer neutral on average, because the plasma has an excess of positive charges due to the absorbed electrons. Due to the large voltage difference, the positive ions are accelerated toward the sample, where they collide with the material and remove it from the surface. The ions can react chemically with the materials on the surface of the samples. Since the sample is etched chemically and the masking material does not react chemically with the ions, the main etching mechanism for the masking material is due to sputtering. [14]

This is the basic principle behind the RIE process. It can be achieved by using a parallel plate reactor. In this type of reactor the sample is placed on top of the electrode, which often leads to direct contact between the sample and the plasma glow. This contact makes a good etch rate but makes the controllability of the etch more difficult. In this type the plasma generation and the bias voltage are linked. Since a high density plasma is required, high RF powers are used, which leads to a heavy ion bombardment and therefore the masking material is etched relatively fast in the parallel plate reactor. This leads to a poor selectivity and if no separate sidewall passivation step is included, the AR is limited to about 2:1 in this reactor type. [14]

The difference between RIE and DRIE reactors can be listed according to etch rate, selectivity, AR capability, and reactor type. Compared to RIE reactors, DRIE reactors have a few different features. They are typically equipped with two RF power generators where the second RF power source controls the bias

voltage. This control of the bias voltage allow the use of low bias voltages which increases selectivity by an order of magnitude. The control of the bias voltage also increases the AR. In DRIE the high-density plasma is often generated by an inductively coupled plasma (ICP) source. When using an ICP source, a plasma density of one to two higher orders of magnitude can be achieved, compared to the parallel plate source, for example from 10^{10} to 10^{12} ions/cm³. This increases the etch rate by approximately one to two orders of magnitude. [14]

By changing the process parameters stated in section 1.4 these six key outcomes can be changed:

- etch rate
- anisotropy
- sidewall angle
- mask selectivity
- substrate selectivity
- etched surface quality

The process parameters are exclusive for the individual structures and must be optimized for particular applications to get the desired product. For example the addition of a passivation step may improve the sidewall profile, but reduce the etch rate, or the decrease in mask selectivity might decrease the etched surface quality by micromasking. All of this is further investigated in the coming sections. [14]

1.3 Deep Reactive Ion Etching in Silicon

This section will investigate the process of creating HAR structures in silicon. It will investigate the Bosch process and some of the basic concepts of the Bosch process. This is done to get a basic understanding of the Bosch process and the finer mechanics of the process.

A DRIE process can be is used to achieve HAR structures. There are two main DRIE process techniques, the Bosch and the cryo-processes. It is only the Bosch process that will be investigated in this report since the cooling needed for the cryo-process was unavailable. The Bosch and the cryo-processes are both fluorine-based techniques. This is done since fluorine-based plasmas for etching silicon offer superior etch rates and higher selectivity than other gasses. However since the fluorine-based plasma is highly chemical reactive, has a spontaneous etching nature, and the silicon fluorine radicals are very volatile, the etch is intrinsically isotropic. To make the etch anisotropic, a sidewall passivation step is introduced to the process. The different DRIE process techniques, that exist, are differentiated by how the sidewall passivation is achieved. The sidewall passivation is crucial to the anisotropy of the etch process. [14]

The compound used for the passivation layer can either be a relatively hard-to-remove or easy-to-remove compound. A hard-to-remove layer can be compounds like silicon oxides or oxyfluorides from silicon surface oxidation. These suffer from some drawbacks since a complete removal of the passivation layer from the trench bottom without leaving layer residues requires energetic ion impacts in combination with added scavenging agents. This reduces the selectivity towards the masking material. The reduced

selectivity makes it difficult to use photoresist as the masking material, to have a high mask selectivity and a trench bottom free from residues, the hard-to-remove passivation layer should be avoided according to Lindroos et al., 2009 [14]. [14]

The easy-to-remove passivation technique is the deposition of polytetrafluoroethylene (PTFE)- or Teflon-like film on the silicon surface. This deposition can be achieved by the generation of $(CF_2)_x$ -type radicals in the plasma. It can be done by starting from octafluorocyclobutane (C_4F_8) or the like, for more see section 1.6. The passivation layer consists of a network of long linear $(CF_2)_x$ chains with little cross-linking, this layer can easily be removed from the surface by low-energetic ion bombardments, without the drawback of residue being left behind, which was the case with the hard-to-remove passivation layer. [14]

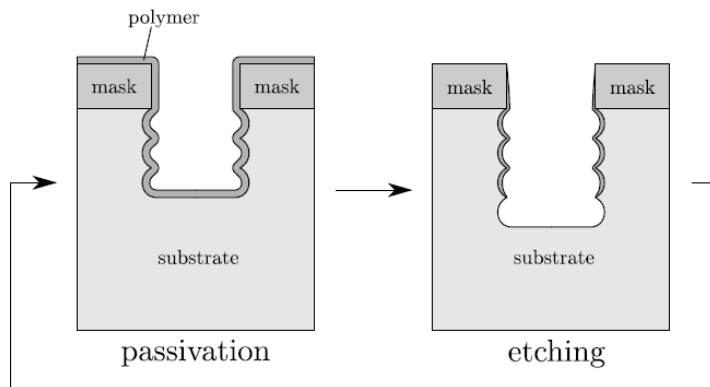


Figure 1.9: An illustration of Bosch process. (left) Sidewall passivation using a $(CF_2)_x$ gas, (right) silicon isotropic etching using SF_6 . [14]

There are two fundamental methods of obtaining sidewall passivation, one is a mixed mode and the other is a pulsed mode. The mixed mode, where the gasses are mixed and the etching and passivation is constant, can be achieved, but it is a challenge to control the passivation and keep the balance between the lateral and vertical etch rates. This was solved by the patented "Bosch process" technology, which is a pulsed mode. The Bosch process is a technique that utilizes the $(CF_2)_x$ -based sidewall passivation technique and the sulphur hexafluoride gas in cycles, for the etching of silicon and achieving HAR structures. Figure 1.9 is an illustration of the process mechanisms.

In the Bosch process, which is a combination of a passivation step and a etching step, the passivation and etching gases are separately feed to the process chamber and introduced to a high density plasma, this is why it is called a pulsed mode. During each passivation step the sample is covered with a thin layer of a Teflon-like film, from the $(CF_2)_x$ gas. The etch step is then initiated by introducing the SF_6 gas to the plasma. During the etching step the Teflon-like film is removed from the sidewall and the bottom. This is done by using the ions in the SF_6 plasma to physically sputter the film away from the surface. Since the ions are accelerated by the electric field, they strike the surface with near normal incidence. The film is therefore not removed from the sidewall and leaves it protected against the fluorine radical. Once the Teflon-like film is removed, at the bottom, the underlying silicon is etched etched by the fluorine radicals. The two step are switched between with regular intervals, like shown in figure 1.9. Removing the Teflon-like film only requires low energy ions this results in a very high mask selectivity, e.g. >150:1 for photoresist.

One of the most important advantage the Bosch process has, is the ability to etches independently of the crystal orientation. We know that wet chemical deep silicon etches will etch along the crystal plane. Where the Bosch process always produces square walls and square channels. The trade-off for etching independent of the crystal plane is an increase in surface roughness. This can be explained by the isotropic nature of the etching gas, which leads to a scalloping of the sidewalls, like seen in figure 1.10. This scalloping of the sidewall surface and how to minimize it will be discussed in section 1.8. [14] [15]

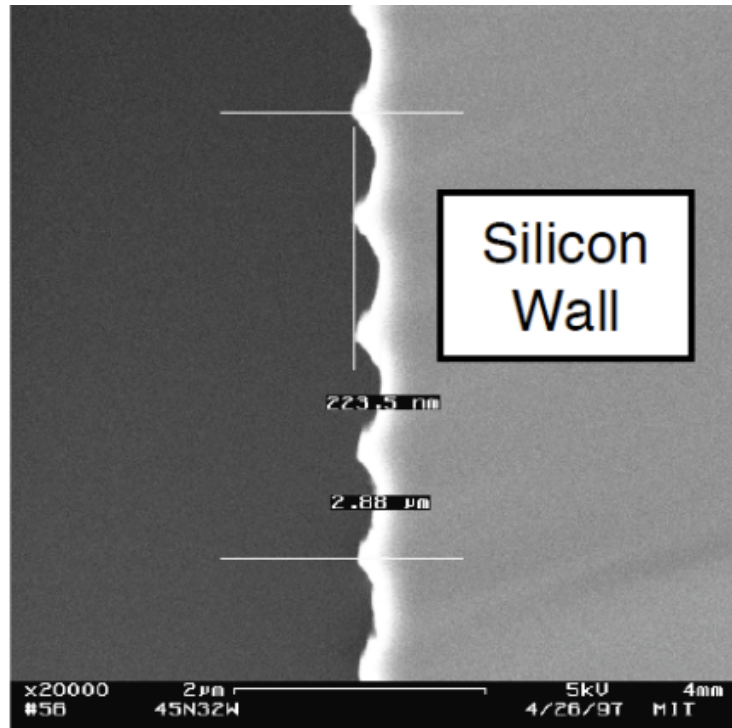


Figure 1.10: Scalloping observed in the walls. This happen due to the isotropic nature of the etching gas. [16]

1.4 Process Parameters

This section will briefly consider each individual variable process parameter, used during the Bosch process. This will help give the reader a basic understanding of the individual parameters before more complicated effects are investigated.

For each structure, the Bosch process is unique. The "perfect" Bosch process is a balance between the "right amount" of polymer on the sidewalls and the bottom of the trench and the duration of the SF_6 etch. Varying either the design or the etch depth, can move the process out of the "perfect window". Whenever a change is made to the structure, the process will need to be modified. The new parameters that create the "perfect window" are found by trial and error. This "perfect window" is more easily found if first the process parameters and their basic influence on the process is understood. [17]

The process parameters can be separated in etch parameters and passivation parameters, these are as follows: **Etch parameters:** Chamber pressure, Etching duration, RF Power, Gas flow rate, Bias voltage, Gas composition.

Passivation parameters: Chamber pressure, Passivation duration, RF Power, Gas flow rate, Bias voltage, Gas composition

Chamber pressure: Chamber pressure controls the amount of gas in the chamber for ionization. This will e.g. affect the anisotropy of the etch. An increase in pressure will give a decrease in anisotropy.

Etch duration: The duration of the etching step controls how long the structure is exposed to the etching plasma. The duration of the etching step has to be long enough, for the polymer at the bottom of trench to be removed, and for the desired depth to be etched. However too long a duration will etch the sidewall passivation and undercut occurs.

Passivation duration: The duration of the passivation step controls how long the structure is exposed to the passivation gas. The longer the duration of the passivation step, the more polymer is deposited to protect the sidewalls.

(Etching) RF power: The influence of RF power is straightforward: an increase in RF power increases both the density and the energy of the free electrons in the plasma.

(Passivation) RF power: The passivation RF power affects the amount of material deposited during the passivation step. The amount increase with the increase in power, but the amount also depend on the gas, e.g. at the same conditions the deposition rate of C_4F_6 vs. C_4F_8 is higher at an increase in power. [12]

Gas flow rate: The flow rates are determined by the desired residency time of the gas in the chamber. That is "how long does the gas reside in the system before it is pumped out". Typically, the residency time should be as short as possible.

Bias voltage: The bias voltage is the potential between the plasma and the negatively charged electrode. It helps determine the directionality of the impending ions. A high bias voltage will guide the ions in a more perpendicular line towards the electrode whereas a lower bias will lead to a higher ion angular distribution (IAD).

Gas composition: Different gas additions will have different influences on the etching and passivation step. This will be investigated in greater detail in the following sections.

The above listed process parameters can have different influences on the outcome. A more specific walkthrough of how the different parameters affect one and other, and how they affect the final product, will be discussed in the following sections. Table 1.17 in section 1.11 is a summary or a guideline on how a change in the process parameters will affect the different outcomes such as etch rate, profile control, and selectivity. [17] [18]

1.5 Etch Mask

This section will investigate different masking materials used for the protection of Si during etching. It will investigate the different masking materials used. This is done to give the reader an overview of the different masking materials and their pros and cons.

When etching, only a certain area is etched to create a structure. This is done by using a mask to protect the material underneath. For silicon there are two types of different masks, there is the soft masks and

the hard masks. The soft mask is a "soft" material, e.g. a photoresist mask and the hard mask is a "hard" material such as SiO_2 or a metal. [14] [17]

The photoresist mask is by far the fastest and simplest mask to use. Typically photoresist thickness ranges from a few 100 nm to hundreds of micrometers, this gives an wide range of etch depth also ranging from a few micrometers to hundred micrometer, depending on the selectivity of the given etching procedure. The photoresist has a drawback, when etching without cooling of the sample, in DRIE reactors, the photoresist is damaged, and the removal of burnt photoresist can be very hard. [14] [17]

Since photoresist has certain limits, hard masks such as SiO_2 , metals, and metal oxides are often used. Hard masks are more durable and offer a higher selectivity than photoresist. This is primarily due to their lack of chemical reactivity with the etch gas molecules and their mechanical strength. The hard masking material adds complexity to the fabrication process, since deposition of a hard mask might include processes such as sputtering, Chemical Vapour Deposition (CVD) combined with thermal oxidation or plating. Some of the most common hard mask materials are SiO_2 , Al, Cr, and Al_2O_3 .

The downside of hard masking materials is the difficult removal of the mask. E.g. aluminium is a good masking material because it is widely available and has a high selectivity in fluorine-based RIE processes. It can be removed in plasma etching by using Cl-based etching, but it is mostly removed using isotropic wet etch, which broadens the original pattern. If the mask is removed using a fluorine-based plasma the aluminium mask is known to create microroughness. Microroughness is created from the sputtering and redeposition of the aluminium to the structure where it acts as a micromask. If photoresist was used as a mask, these complications are avoided. So it all really comes down to how deep the etch is supposed to be and whether or not the temperature is controllable. [14] [17]

The metals most commonly used as hard masks are Cr and Al. Al is used due to the extremely high selectivity towards Si (100 000:1). The downside is, at relatively low ion energies (<40 eV) the material is easily eroded, and this gives rise to an increase in surface roughness for the Si in close proximity to the mask. Where as Cr has a lower selectivity, but it has the upside that even at relatively high ion energies (200 eV) the mask is experiencing minimal erosion. [19]

1.6 Passivation Step

The Bosch process is a time multiplexed process which is composed of two steps, namely an etch step and a passivation step. This section will investigate the passivation step by looking at the gas composition and its influence.

As we know most dry etchings of silicon is done by using fluorine free radicals. These are created from the fluorine containing gases and by forming volatile SiF_4 during the etch the material is removed. Fluorine plasma reacts with silicon spontaneously. The use of fluorine results in a high etch rate, but it produces profiles that are isotropic. [20]

Often the fluorine is combined with carbon to produce polymer deposition using the CF_x gas. The CF_x film growth is dependant on certain factors such as F/C ratio and the presence of other gasses, but also the same as a normal plasma i.e. RF power and chamber pressure.

Oxygen can be added to the silicon etching. At a concentration of less than 16% the oxygen reacts with C to create CO, CO_2 , this increase the F/C ratio and eliminates the film growth.

Hydrogen on the other hand decrease the F/C ratio, thus increase film growth. Factors that tend to have the

biggest impact on polymerization (film growth) and selectivity are temperature, hydrogen concentration, pressure, and ion bombardment.

The F/C ratio in dry etching is a key parameter to controlling the etching. With an F/C ratio >3 etching is dominant and with an F/C ratio <2 a Teflon-like film is created. This can be seen in figure 1.11. The reason for a movement towards an etching dominance is due to increased bias voltage caused by the enhanced energy of the ions striking the surface. This results in polymer sputtering and thus etching becomes more dominant. When etching silicon, no oxygen is released and F is consumed thus lowering the F/C ratio and increasing polymerization. A lowering of the bias voltage in the right regime will enhance polymerization, this can be done by increasing the pressure, however this will decrease the anisotropy, since the anisotropy is highly dependable on the direction of the ions. [20] [21]

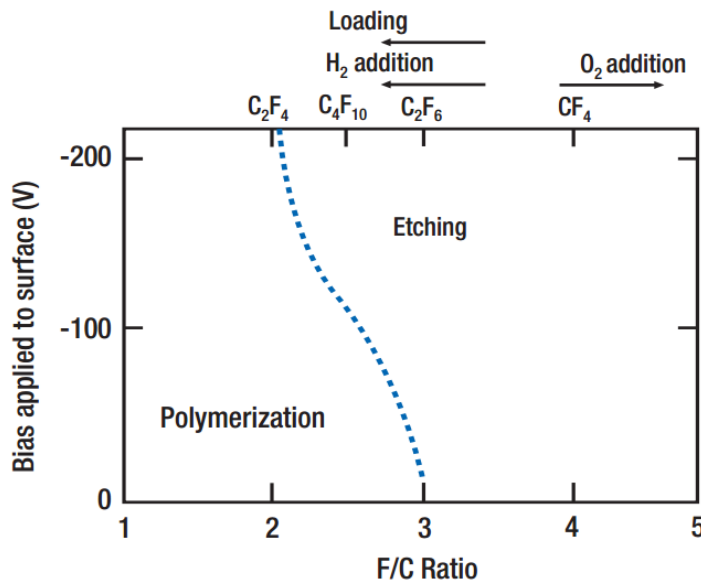


Figure 1.11: A control graph for Si RIE etching in a CF_x environment. It shows the influence of fluorine to carbon (F/C) ratio compared to electrode bias voltage. [20]

1.7 Etch Rate

Etch rate is changed by a lot of things, the main reasons for a change in etch rate can be assigned to the changes in a single recipe. Etch rate changes can also be assigned to change in the environment. This section investigates etch rate, etch rate of the masking material, and etch rate uniformity.

The etching process of silicon consists of three components: physical sputtering, spontaneous thermal etching, and ion-enhanced chemical reaction. Where the ion-enhanced chemical reaction is the component with the most impact. The etch rate is the speed with which the material is etched, this is measured in $\mu\text{m}/\text{sec}$. Changing the process parameters of the etching cycle will obviously change the etch rate. Eg. decreasing the passivation duration will result in higher etch rates, due to thinner passivation layer. Similarly changes in etch gas flow rate and etch durations will also affect the etch rate. There are in fact 9 factors that will influence the etch rate. [12] [14] [16]

They include:

- Etch gas flow rate
- Duration of the etching step
- Passivation gas flow rate
- Duration of the passivation step
- RF power during etch
- RF power during passivation
- Temperature
- Chamber pressure
- Gas composition

These factors affect the recipe in different ways. Understanding how these factors effects the etch rate, give an idea of how to change them to achieve a desired etch rate and control individual parameters parameters. Some changes are more obvious than others, e.g. increase in the RF power during etch increases the amount of radical production in the plasma, which in turn leads to a higher etch rate. However, for low etch gas flow rates the change in RF power only have a reduced effect on the etch rate, since there isn't enough radicals in the plasma to affect, but as the flow rate increases the etch rate increases with the increase in RF power and flow rate.

A change in chamber pressure will change the number of collisions in the plasma by changing the atomic fluorine concentration which increase the etch rate. However increasing pressure a lot, results in an etch rate decrease. This is due to ion energy and radical flux decrease in high pressure plasma leading to a decrease in etch rate.

The etch rate also varies according to the duration of the etching step, due to a longer exposure to the etching plasma. The etch rate decreases, with the increase of the duration of the passivation step, since a longer duration leads to the deposition of a thicker Teflon-like film. [12] [14] [16]

The etch rate is dependant on the amount of etch able area, this effect is called the loading effect. The etch of silicon in a plasma environment is a chemical reaction so a larger etch able area leads to a lower reactant supply and consumption balance. When etching a small area the gas flow can supply enough reactant species, but if the area is to large not enough reactive species can be supplied. This can be solved by increasing the flow rate. However this is not always a good idea since it can result in a loss in sidewall profile control. [14]

Etch Rate of The Masking Material

Selectivity is an important parameter, it is the relative silicon etch rate with respect to the etch rate of the masking material, i.e. the etch selectivity. This is important since if the mask is etched through before the desired depth is reached then the top of the structure will be damaged. So it all depends on the etch rate of the masking layer.

The etch rate of the masking layer is not to be confused with the etching of the passivation layer. The etch rate of the masking layer is dependent on the masking layer material, but there are still some fundamental things that influence both the soft and the hard masking material. In general a low etch rate in the masking

material is desired to achieve a HAR structure. The masking etch rate is in general sensitive towards bias voltage, pressure, and the duration of the etching and passivation steps. The masking etch rate increases with applied bias voltage, that increases the ion bombardment energy, thus increases the anisotropy but lowers the selectivity.

If the pressure is increased the masking etch rate decreases, but this increases the sputtering and redeposition of the masking material, which promotes the formation of "micrograss" or microcolumns.

The duration of the passivation step is a determining factor in the etch rate of the masking material. If the duration of the passivation step is long, more polymer is deposited on the structure, thereby protecting it from the etching plasma for a longer time. Similarly the duration of the etching step is a determining factor, since the longer the time the mask is exposed to the etch the more material is etched. [14] [16]

Etch Rate Uniformity

Etch rate uniformity is important since all factors that affect the etch rate can change the etch rate uniformity. The plasma density is for instance higher in closer proximity to the power source, this result in an increase in locale etch rate. This shows that the etch rate uniformity is highly dependable on reactor design. Parameter changes that might improve the etch rate uniformity, are e.g. passivation gas flow rate, etch gas flow rate, and temperature control. E.g. an increase in passivation flow rate and a decrease in etch gas flow rate may improve etch rate uniformity, but at the expense of the overall etch rate. The local concentration of reaction radicals, i.e. atomic fluorine concentration, also affects the etch rate uniformity. According to Ayón et al. [16], a low SF₆ flow rate is beneficial for the etch rate uniformity. This can be explained by the pressure changing as the flow rate changes. A lower pressure improves etch rate uniformity because the diffusivity varies inversely with the pressure, and greater diffusivity provides a better distribution of the ion flux at the sample. However it is not only the ion flux that is better, but also the flux of the products, or neutral reactants, is increased, which produces a more uniform flux at the sample. This require a low flow rate, but to achieve high etch rates and reduce ARDE a high flow rate is required. So the importance of etch rate uniformity depends on the individual structures.

The etch rate is less uniform when the pressure or average loading is increased. Adding a small amount of oxygen can help improve etch rate uniformity. Inert gases such as argon and helium help stabilize the plasma, enhance anisotropy, and improve etch rate uniformity, but it also reduce the etch rate by dilution. [12] [19]

1.8 Profile Control

Profile angle and surface roughness are very important for most applications. This section will investigate what parameter affect the profile and the scalloping of the structure. This section will also investigate how to minimize and otherwise control these two effects.

The ability to create and control the profile, regardless of the crystal orientation, is one of the major advantages created by the Bosch process. In general a smooth and straight profile is desired in HAR silicon structures, but a sloped profile angle (e.g. around 85°) can be desired, this can be achieved using the Bosch process. The profile angle is strongly influenced by the RF power and the ratio between the duration of the etching and passivation steps. Where a too short duration of the etching step leads to a positive slope and the other way around. A SEM picture of a positive slope can be seen in figure 1.12d. A too short duration of the etching step will remove the passivation film completely, this will lead to an increase in surface roughness and other undesirable effects such as micromasking and micrograss

formation. Not all structures will produce the same profile angle with the same process parameters. Profile angle that changes with structure size is a known issue. If the process is optimized to give a vertical profile on a certain structure, then structures larger than the original structure may have a re-entrant profile, while ones smaller than the original structure will have a positive profile angle. This phenomenon may be reduced by changing process parameters such as chamber pressure in order to achieve vertical profiles. [12] [14] [19]

The sidewall can have different shapes as seen in figure 1.12. These profiles are obtained due to different reasons. The first profile seen in figure 1.12a is a result of ion bombardment. This is seen when the sharp corners of the mask is eroded due to sputtering. If the mask is sputtered significantly then the bottom edge will move inwards, making the profile larger, and the feature will develop a tapered profile. This effect is called bowing of the sidewall.

The formation of microtrenches is an effect often seen in microstructures. Microtrenches are small trenches at the sidewall, at the bottom of the trench, see figure 1.12b. The formation of microtrenches is an undesired effect. This is caused by the impinging ions that are striking the surface at a near perpendicular angle, however there is a small lateral component that affect the profile. This can in some cases lead to a specular reflection of the vertical sidewall, which increases the local concentration of ions, near the bottom of the trench and causes microtrenching.

Figure 1.12c is the phenomena called undercutting or undercut, it is a result of isotropic etching. It is caused, in the case of dry silicon etching, by the chemical attack of SF_6 which etches isotropic by nature. It is possible to minimize the undercut by increasing the bias or use sidewall protection. These are the four fundamental undesirable profiles, created during plasma etching. [12] [22]

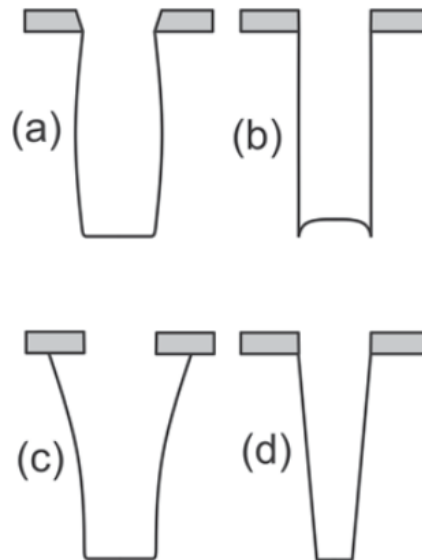


Figure 1.12: A sketch of various profiles: (a) bowing profile due to mask erosion (b) microtrenching due to enhanced ion flux at the bottom (c) undercutting is the product of isotropic etching. (d) positive profile is a product of long duration of the passivation step. [22]

Sidewall Scalloping

As a result of the Bosch process the sidewalls are not perfectly smooth. They have a scalloped shape, as seen in figure 1.10. The shape of the scallops is a function of the operating conditions. According to Ayón et al. [16] scallops as low as 50 nm can be achieved under the right conditions, without losing control of the profile angle. It can be further reduced to 10 nm by optimizing the duration of the etching and passivation steps, but at the expense of the sidewall profile angle. Ayón et al. [16] observed that in general a higher RF power to pressure ratio and a shorter etching cycles tend to produce smoother walls. Another solution, in the attempt to reduce sidewall scalloping, is to use ultrafast passivation gas pulses (100ms), and use fast etch cycles (1-2s), this will result in hardly any scalloping ($\ll 10\text{nm}$), as can be seen in figure 1.13. The drawback of the ultrafast process is the increase in micromasking and surface containments, which increase the surface microroughness at the bottom. This microroughness may increase the micrograss and other residue formations.

Sidewall scalloping can be treated after the Bosch process is done, by wet etching using KOH and IPA. This has been shown to reduce the scalloping from 50 nm to 6 nm, but this process is complicated. [12] [16]

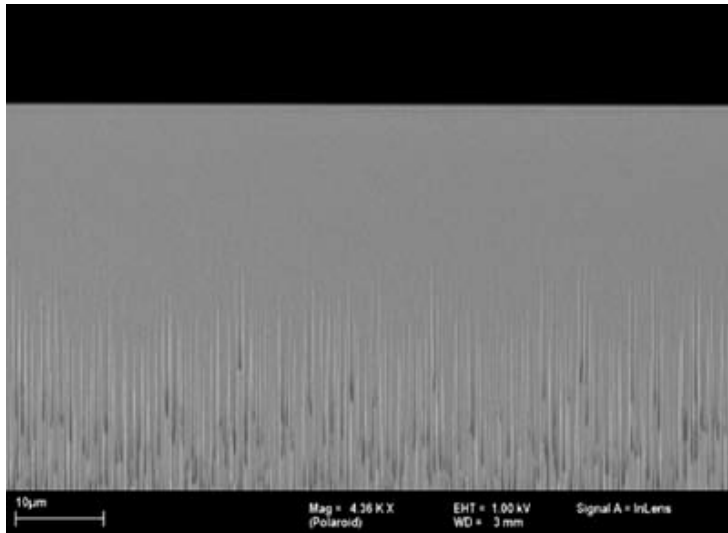


Figure 1.13: A SEM picture of a sidewall which was fabricated using the ultrafast Bosch process parameters. Hardly any horizontal scalloping is visible, but some vertical impurities are visible, this indicates the beginning of microroughness formations. [14]

1.9 ARDE and RIE Lag

This section will investigate the phenomenon called Aspect Ratio Dependant Etch. This is done to better understand how to counter the problem.

Aspect Ratio Dependant Etch (ARDE), is an effect that occur in all etch processes, but it is of great concern when fabricating HAR structures. The effect is observed by a decrease in etch rate as the AR increases, which indicates that ARDE is a dynamic effect. RIE lag, compared to ARDE, is a static effect. It refers to the observation that small features are not as deep as large features. So RIE lag can be directly observed, see figure 1.14, and ARDE is an effect that increases as the AR increases. Both

effects depend on the fact that, reactant and product transport to and from HAR structures is limited, by gas dynamics in narrow features. So in the case of silicon etching, the main reason for ARDE, is the depletion of fluorine radicals at the trench bottom. The process parameters that are dominant is SF_6 flow rate, pressure, temperature, and directionality of the ion flow. [12] [14]

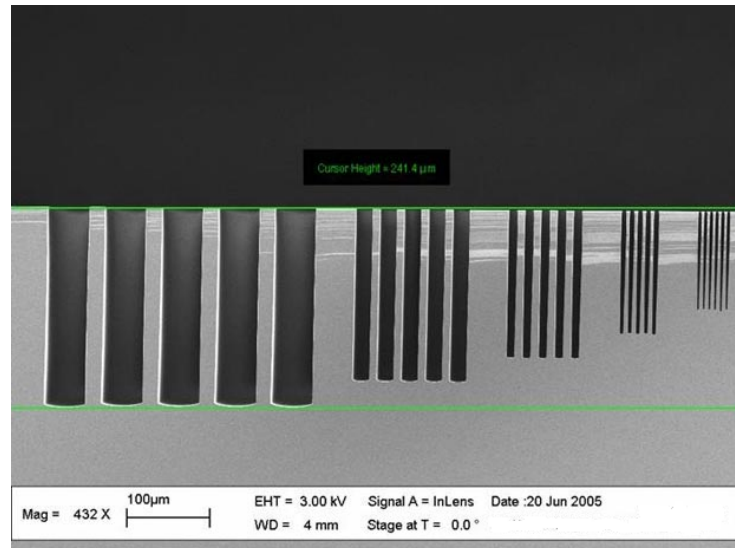


Figure 1.14: A DRIE in silicon that clearly show a dependence between AR and etch rate. [23]

ARDE is a result of transport phenomena. So a method to overcome ARDE is to change the process parameters as the etch progresses. Increasing the bias voltage as the process progresses, has been shown to have a positive effect on the ARDE. Since ARDE is also dependant on the pressure, it was shown by W. H. Juan and S. W. Pang [24] that a lower pressure tends to tighten the IAD, thereby improve the mass transfer at the bottom of the trench and the ARDE. [12] [14]

The maximum AR of a given structure can be simulated, it is called the "critical aspect ratio". It can be seen from figure 1.15 that for a given set of parameters the etch rate will drop to zero at the critical AR. There is some maximum achievable AR for all structures. [12] [14]

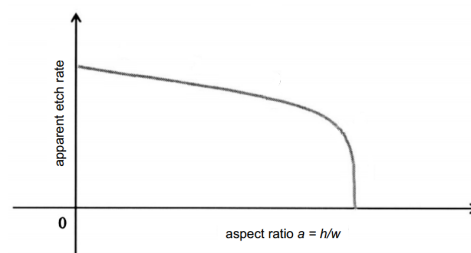


Figure 1.15: A sketch of the relation between AR and etch rate. It is clear that the etch rate drops to zero at the "critical aspect ratio". [12]

Lindroos et al., [14] studied the three stages of the Bosch process, namely the polymer deposition, the polymer etch, and the silicon etch. They concluded that the deposition and the silicon etch are dependant on the AR of the structure. They also concluded that the polymer etch rate is almost independent of the

feature dimensions. The achievable AR can be improved by adjusting the gas composition. To improve the achievable AR, a more efficient removal of the passivation film at the bottom of the trench can be achieved by changing the gas composition, e.g. by adding Argon. [12] [14]

1.10 Micrograss

Micrograss, microcolumn or black silicon³ is an effect that happens as a result of the sputtering and re-deposition of masking material and other residue, that creates micromasking sites. Micromasking sites at the bottom of the trench promotes the formation of micrograss see figure 1.16. There are different ways to overcome the micrograss formation. One way is to increase the bias voltage, thus removing the polymer at the bottom of the trench, but increasing the bias voltage might increase the etch of the passivation layer on the sidewalls and thus creating a bowing shaped profile.

The SF₆ flow rate also affect the formation of micrograss. Dixit and Miao, [25] did an extensive research regarding the connection between flow rate and formation of micrograss. They concluded that an increase in flow rate increases the formation of micrograss. They also investigated the ratio of passivation to etching duration and discovered that there is an optimum ratio which creates a grass free bottom trench. This is concurrent with other studies in the field which suggest that the micrograss formation can be minimized or eliminated all together by increasing the etching step duration, but also other parameters have an effect on the formation of micrograss, such as, RF power, temperature, and pressure. E.g. according to Lindroos et al., [14] high temperatures enhance the removal of micrograss.

But apart from the process parameters, the formation of micrograss is more prominent in larger features sizes. This makes sense since small features compared to open areas are less likely to experience the redeposition of the passivation layer, thus less likely to experience the formation of micromasking sites. [16] [25]

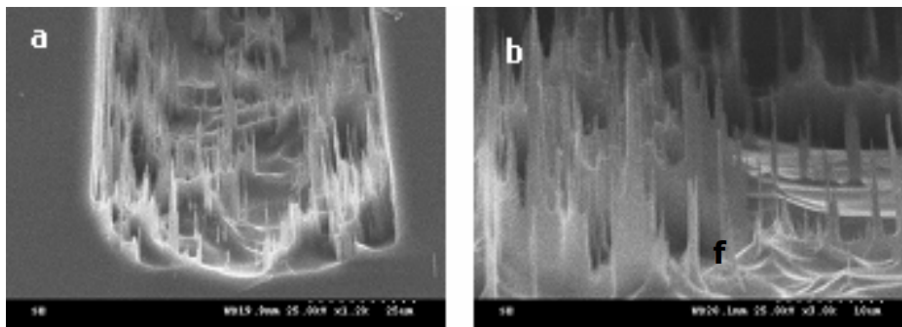


Figure 1.16: SEM picture of bottom micrograss formations in a trench etched at an SF₆ flow rate of 400 sccm. [25]

1.11 Resume

This section contains a table, table 1.17, which is a compression of some of the info from the previous sections. The purpose of this table is to give the reader a quick help guide to fabricating HAR structures using the Bosch process.

³It is called black silicon since it will appear dark when visually inspected.

| Increase Response | SF6 Flow | C3F8 Flow | Power | Pressure | Passivation duration | Etching duration | Bias Power |
|---------------------|----------|-----------|-------|----------|----------------------|------------------|------------|
| Etch Rate | ↑ | ↔ | ↑ | ↑ | ↓ | ↑ | ↑ |
| Mask Selectivity | ↔ | ↔ | ↓ | ↑ | ↑ | ↓ | ↓ |
| Uniformity | ↑ | ↔ | ↔ | ↓ | ↔ | ↔ | ↔ |
| Profile Angle* | ↓ | ↔ | ↓ | ↓ | ↑ | ↓ | ↓ |
| ARDE Variation | ↓ | ↔ | ↔ | ↑ | ↔ | ↔ | ↑ |
| Sidewall smoothness | ↓ | ↑ | ↓ | ↓ | ↑ | ↓ | ↓ |

| | |
|-------------------------------------|--------------------------------------|
| ↑ Strong increase in response | ↔ Little or no effect in response |
| ↓ Strong decrease in response | ↑ Increase in response |
| | ↓ Decrease in response |

*Figure 1.17: The diagram presents the typical first order effects of the Bosch process. *: Arrow down: negative profile, Arrow up: positive profile*

The diagram only contains first order effects, e.g. we know that an increase in pressure will increase the masking selectivity (as seen in the diagram), but the diagram does not tell the reader that this will lead to an decrease in micrograss formation which is a second order effect. The diagram is meant as a "rule of thumb", to be used when fine tuning the Bosch process.

1.12 Project Goal

The focus of this project is to fabricate a GRIN lens structure based on the design proposed by Brincker and Karlsen, [1] using the Bosch process. Since the Institute of Physics and Nano Technology have no prior experience in the fabrication of microstructures, using the Bosch process, the Bosch process have to be optimized to the fit the RIE system. The GRIN structure needs to be integrated directly on the PCA substrate therefore the material used for fabrication the lens will be silicon. This project will investigate the possibility of fabricating deep trenches with near vertical sidewalls.

The lens structure will be fabricated utilizing the Bosch process. This will require the knowledge on how to use lithography, e-beam lithography, lift-off method, metal deposition, and RIE.

Experimental Procedure 2

This section will describe the process of the four optimization rounds involved in the optimization and fabrication of the lens structure. After this the RIE system will be described, afterwards the process parameters of the individual samples will be listed.

The Institute of Physics and Nanotechnology have no prior experience in the field of etching HAR microstructures, less in using the Bosch process.

The optimization of the Bosch process is divided into four optimization rounds; first an optimization round of the two process steps, second an optimization round involving a large linear structures, third an optimization round of a designed linear structure using, fourth an optimization round of the lens structure.

The main fabrication technique of the samples, rely on the same 5 basic steps; deposition of resist layer, exposure and removal of the exposed resist, deposition of Cr, lift-off, and etching of the wafer. This can be seen in figure 2.1.

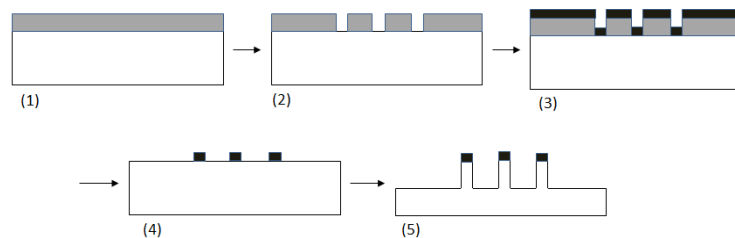


Figure 2.1: Sketch showing the five basic fabrication steps. (1) is the deposition of resist layer, (2) is exposure and removal of the exposed resist, (3) is deposition of Cr, (4) is the lift-off procedure, (5) is etching of the wafer.

2.0.1 First optimization round

The Bosch process was first optimized by investigating the two process steps separately. The etching step was investigated by using SF_6 . The etch depth was found by placing two displaced wafers on top of each other, this was done to protect the bottom wafer. The etch depth was then measured using the profiler.

The passivation step was optimized in the same way, the C_3F_8 gas was chosen and two displaced wafers were placed on top of each other. The thickness was measured using the profiler.

2.0.2 Second optimization round

The samples created during the first optimization round (sample 1–12) were created in the following way: a 1x1 cm silicon wafer was cleaned using a Martin Walter Powersonic ultrasonic tank. The sample was first exposed to ultrasound in acetone for 1 minute, then water for 1 min, and then ethanol for 1 min. Afterwards the sample was spin coated with photoresist S1813 at 2500 rpm for 1 minute, and baked at 110 °C for 1 min. The sample was then exposed to an UV light source¹, for 90 seconds, and then developed in a Micro developer for 1 min. The structure was then coated with Cr in a SVS 2400 sputter coater, using the variables found in appendix A. The sample was submerged into acetone to remove resist and do the lift-off. This concludes the preparation of the sample, the next step is etching.

The mask used during the second optimization round consisted of trenches with different widths. The exposed silicon is approximated to 55%.

Second passivation test

Due to the difficulty in creating a passivation layer the passivation process was tested again. This test was carried out during the second optimization round. The process was tested by placing a single wafer in the process chamber and then after depositing the passivation layer for three minutes, the thickness was measured using an ellipsometer.

2.0.3 Third optimization round

The samples created during the third optimization round (sample 13–17), were created in the following way: a 1x1 cm silicon wafer was cleaned using a Martin Walter Powersonic ultrasonic tank. The sample was first exposed to ultrasound in acetone for 1 minute, then water for 1 min and then ethanol for 1 min. The sample was afterwards spin coated with PMMA 3% at 2000 rpm for 1 min and baked at 110 °C for 1 min. The sample was then exposed in a Zeiss EVO 60 scanning electron microscope using the Raith Elphy Plus system, for the detailed process of the preparation the SEM for e-beam writing see [26]. Afterwards the sample was submerged in a developer for 30 sec and then a stopper for 15 sec. The structure was then coated with Cr in a SVS 2400 sputter coater, using the variables found in appendix A. The sample was submerged into acetone to remove resist and do the lift-off. This concludes the preparation of the sample, the next step is to etch the sample.

The structure, used during the third optimization round, consisted of trenches with different widths, ranging from 2 μm to 25 μm . Figure 2.2 shows a sketch of the comb structure used during the second optimization round.

¹Isel UV-belichtungsgerat

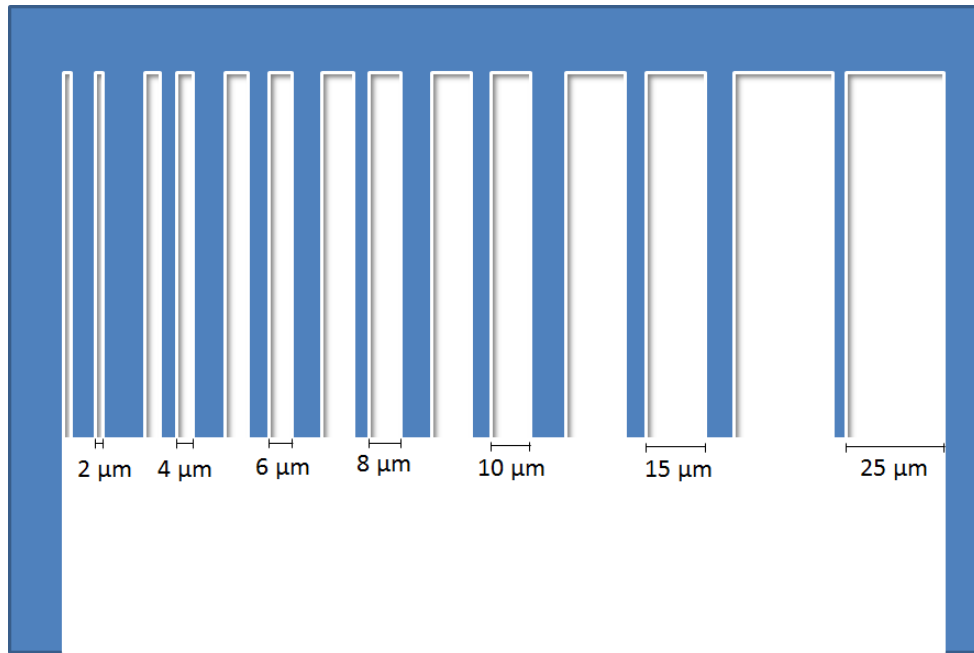


Figure 2.2: Sketch showing the comb structure as seen from above.

2.0.4 Fourth optimization round

The wafer with the lens structure (sample Lens1) was created in the following way: a 1x1 cm silicon wafer was cleaned using a Martin Walter Powersonic ultrasonic tank. The sample was first exposed to ultrasound in acetone for 1 minute, then water for 1 min and then ethanol for 1 min. The sample was then spin coated with PMMA 3% at 2000 rpm for 1 minutes and baked at 110 °C for 1 min. Afterwards the sample was exposed in a Zeiss 1540 XB scanning electron microscope using the Raith Elphy Plus system, the preparation of the SEM is the same as for the EVO 60 SEM [26]. The sample was then submerged in a developer for 30 sec and a stopper for 15 sec. The structure was then coated with Cr in a SVS 2400 sputter coater, the individual parameters can be found in appendix A. The sample was submerged in acetone and exposed to ultrasound do the lift-off. This concludes the preparation of the sample, the next step is to etch the sample.

The exposed silicon is approximately 99.9%.

2.0.5 RIE system and parameter control

The etching of the structures were carried out using a Surface Technology Systems 320 PC RIE. It is a RIE system using a capacitively coupled plasma. The process chamber is made from aluminium and have a diameter of 343 mm and a hight of 144 mm. The sample holder is 300 mm.

The equipment have 8 different gas delivery channels. The gasses available were; CHF₃, O₂, CF₄, He, C₃F₈ and SF₆.

The equipment included one 13.56 MHz RF power source. This means that the bias voltage has to be controlled by changing the other process parameters.

The process parameters that were variables were:

Etch parameters: Pressure, Etch duration, RF Power, Flow rate, Gas type

Passivation parameters: Pressure, Passivation duration, RF Power, Flow rate, Gas type

Pressure: The pressure can be operated in two ways, one where there is a predetermined pressure for both etching and passivation cycle, or with a fixed angular position for the automatic pressure control (APC). In the case of the fixed APC, the pressure is determined by the gas flow rate. The results presented in this report uses the first approach.

The specific process parameters for the individual etching processes can be found in table 2.1 and 2.2.

A sketch of the etching chamber can be seen in figure 2.3.

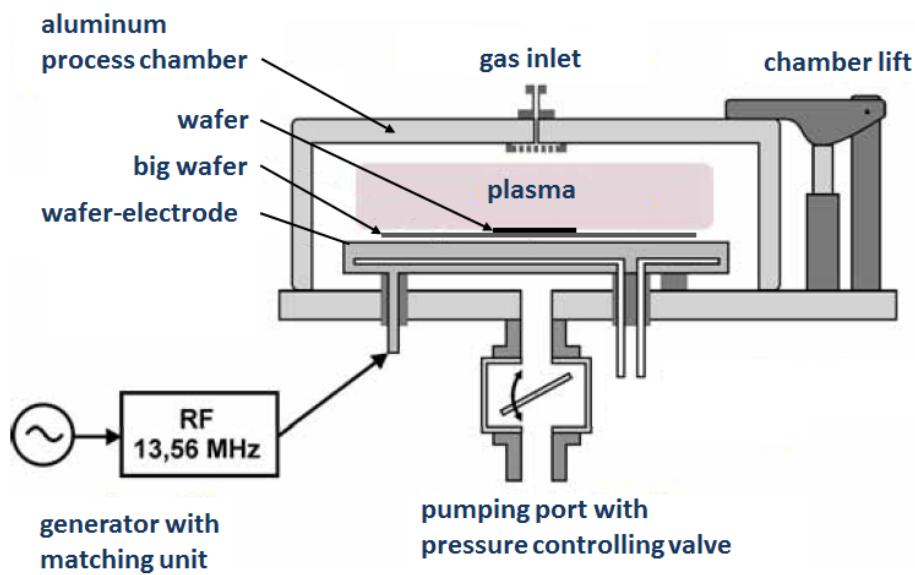


Figure 2.3: Sketch of the etching chamber. Modified from [27]

The Bosch process requires a cycle of etching and passivation steps. These were run almost continuously. A graph showing the cycle can be seen in figure 2.4. This show how there is a gas overlap when switching between the passivation gas and the etching gas.

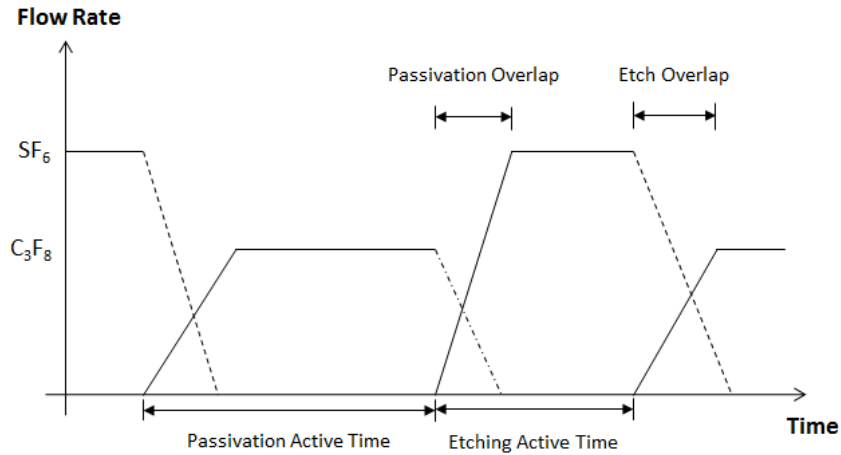


Figure 2.4: Graph showing the gas flow cycle during the etching step and the passivation step. The overlap is caused by a loading of the process parameters in the RIE software.

When individual passivation and etching steps works then the "perfect" process parameters can be found in the following trail-and-error way:

1. Make sure that the chamber is "stable". Cleaning of the reactor chamber should be done before the system has been used for more than 6 hrs.
2. Run the etch and check the profile angle. If it is $<90^\circ$ then increase the deposition time by 20 sec, if it is $>90^\circ$ then decrease the deposition time by 20 sec. This step is repeated until the desired profile is found.
3. The change in passivation duration does not have to be a full 20 seconds, but can be less to obtain the desired profile.

2.0.6 Investigating the samples

To investigate the samples an Ambios XP-2 profiler and a Zeiss EVO 60 SEM were used.

The profiler was used to measure the height variation of the samples, and using the data to calculate the etch rates. The Ambios XP-2 profiler can measure height variations of up to 400 micrometers.

2.0.7 Process parameters

| Process | Etch Step | | | | Bias (V) | Time (s) | Etch rate ($\mu\text{m}/\text{min}$) | # of cycles |
|-----------|------------------|-----------------|------------------|---------------------|----------|----------|--|-------------|
| | Pressure (mTorr) | Gas | Flow rate (sccm) | RF Power Source (W) | | | | |
| Sample 1 | 150 | SF ₆ | 70 | 300 | 20 | 10 | 0.92 | 40 |
| Sample 2 | 150 | SF ₆ | 70 | 300 | 20 | 10 | 0.97 | 104 |
| Sample 3 | 150 | SF ₆ | 70 | 300 | 20 | 10 | 0.74 | 86 |
| Sample 4 | 150 | SF ₆ | 70 | 300 | 20 | 10 | 0.1 | 84 |
| Sample 5 | 150 | SF ₆ | 70 | 300 | 20 | 10 | 0.19 | 70 |
| Sample 6 | 150 | SF ₆ | 70 | 300 | 20 | 10 | 0.12 | 84 |
| Sample 7 | 150 | SF ₆ | 70 | 300 | 21 | 10 | 0.13 | 84 |
| Sample 8 | 100 | SF ₆ | 50 | 300 | 40 | 10 | 0.13 | 84 |
| Sample 9 | 100 | SF ₆ | 50 | 300 | 50 | 10 | 0.45 | 42 |
| Sample 10 | 100 | SF ₆ | 50 | 300 | 50 | 10 | 0.29 | 21 |
| Sample 11 | 100 | SF ₆ | 50 | 300 | 50 | 10 | 0.16 | 21 |
| Sample 12 | 100 | SF ₆ | 50 | 300 | 50 | 10 | 0.09 | 21 |
| Sample 13 | 100 | SF ₆ | 50 | 300 | 50 | 10 | 0.04 | 63 |
| Sample 14 | 100 | SF ₆ | 50 | 300 | 50 | 10 | 0.07 | 105/336 |
| Sample 15 | 100 | SF ₆ | 50 | 300 | 50 | 10 | 0.09 | 147 |
| Sample 16 | 100 | SF ₆ | 50 | 300 | 50 | 10 | 0.06 | 399 |
| Sample 17 | 100 | SF ₆ | 50 | 300 | 50 | 10 | 0.1 | 147 |
| Lens 1 | 100 | SF ₆ | 50 | 300 | 50 | 10 | 0.12 | 147 |

Table 2.1: Table of the parameters used during the etching step for the individual samples.

| Process | Passivation Step | | | | Bias (V) | Time (s) | Depth (μm) | Mask |
|-----------|------------------|-------------------------------|------------------|---------------------|----------|----------|-------------------------|------|
| | Pressure (mTorr) | Gas | Flow rate (sccm) | RF Power Source (W) | | | | |
| Sample 1 | 150 | C ₃ F ₈ | 50 | 300 | 170 | 7 | 20 | Cr1 |
| Sample 2 | 150 | C ₃ F ₈ | 50 | 300 | 170 | 14 | 65 | Cr1 |
| Sample 3 | 150 | C ₃ F ₈ | 50 | 300 | 170 | 25 | 51 | Cr1 |
| Sample 4 | 150 | C ₃ F ₈ | 50 | 300 | 170 | 90 | 15.5 | Cr1 |
| Sample 5 | 150 | C ₃ F ₈ | 50 | 300 | 170 | 25 | 9.3 | Cr2 |
| Sample 6 | 150 | C ₃ F ₈ | 50 | 300 | 170 | 25 | 8.2 | Cr2 |
| Sample 7 | 150 | C ₃ F ₈ | 50 | 300 | 170 | 25 | 8.8 | Cr2 |
| Sample 8 | 200 | C ₃ F ₈ | 50 | 250 | 70 | 25 | 9 | Cr2 |
| Sample 9 | 200 | C ₃ F ₈ | 50 | 250 | 75 | 25 | 15.7 | Cr2 |
| Sample 10 | 200 | C ₃ F ₈ | 50 | 250 | 75 | 50 | 7.4 | Cr2 |
| Sample 11 | 200 | C ₃ F ₈ | 50 | 250 | 75 | 80 | 5.8 | Cr2 |
| Sample 12 | 200 | C ₃ F ₈ | 50 | 250 | 75 | 120 | 4.3 | Cr2 |
| Sample 13 | 200 | C ₃ F ₈ | 50 | 250 | 75 | 120 | 5.7 | Cr2 |
| Sample 14 | 200 | C ₃ F ₈ | 50 | 250 | 75 | 100 | 15/? | Cr3 |
| Sample 15 | 200 | C ₃ F ₈ | 50 | 250 | 75 | 80 | 23 | Cr3 |
| Sample 16 | 200 | C ₃ F ₈ | 50 | 250 | 75 | 100 | 48 | Cr4 |
| Sample 17 | 200 | C ₃ F ₈ | 50 | 250 | 75 | 100 | 16.7 | Cr5 |
| Lens 1 | 200 | C ₃ F ₈ | 50 | 250 | 75 | 100 | 20 | Cr4 |

Table 2.2: Table of the parameters used during the passivation step for the individual samples.

Results and Discussion 3

3.1 Results

This section will show the results from the optimization of the Bosch process. It will be divided into the four categories that are: first, second, third, and fourth optimization round.

3.1.1 First optimization round

The first step was to investigate and optimize the etching step of the Bosch process. According to Wu et al., 2010 [12] the most used gas for etching Si is SF₆, therefore SF₆ was chosen as the gas to be used during the rest of the experiments. Figure 3.1 shows the connection between etch rate, flow rate of SF₆, and RF power. This was done to investigate the effect of these parameters on the plasma and the etch rate. The plasma was stable at all RF powers and did not show signs of flickering or instability. This concluded the investigation of the etching step for a silicon wafer without the passivation step.

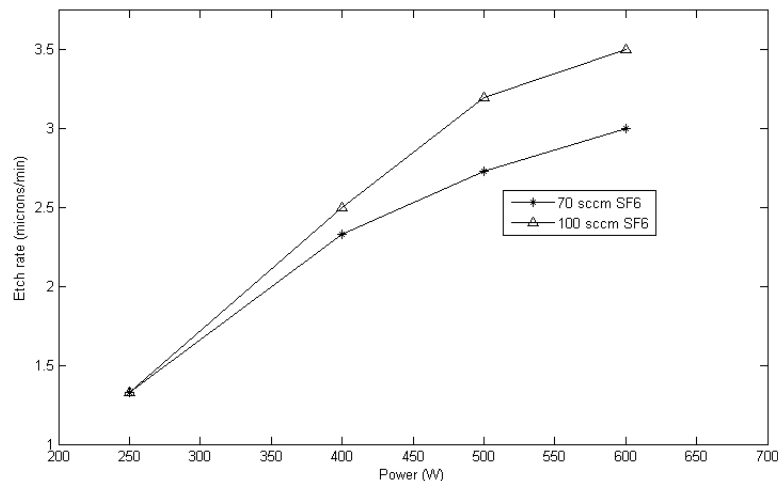


Figure 3.1: *The etch rate was determined on silicon using only the etching step. The pressure was kept at 150 mTorr at all times.*

Based on Wu et al., 2010 [12] the most used gases, for a successful passivation step, were identified to be C_4F_8 and C_4F_6 . However these gases were not available, so C_3F_8 was used as the passivation gas, for this project. The investigation of the passivation step, was to determine the deposition time of the passivation layer, and the stability of the plasma according to RF power. The results showed a deposition rate of 2-3 nm/min¹ at a RF power of 150 W and a reasonable stability of the plasma with an RF power below 300 W. For the remainder of this project, the RF power during the passivation step was kept below 300 W to avoid flickering and instability of the passivation plasma. This concluded the investigation of the passivation process and of the first optimization round.

¹The deposition rate was later discovered to be the etch rate of the material.

3.1.2 Second optimization round

The goal of the second optimization round was to attempt to reproduce and optimize the Bosch process, utilizing the RIE system available. The starting values for sample 1 was chosen based upon the experience gained during the first optimization round, the limitations of the RIE system, and some process parameters found by Wu et al. [12], Ayón et al. [16], and Chen et al. [28]. The process parameters can be found in table 2.1 and 2.2.

The reason behind the similarities in the process parameters, for the etching and passivation step, is due the fact that it was believed, that a large change in process parameters would result in a less stable plasma. Sample 1 showed a large amount of undercut (was not measured). To reduce this undercut, the duration of the passivation step was increased. This was done since the amount of passivation layer, on the sidewalls, is what inhibits the SF_6 from etching the sidewalls and increasing the amount of undercut.

Sample 2 also showed a large undercut ($23.7 \mu\text{m}$ undercut). The undercut was expected to be much less, in the range of $1\text{-}2 \mu\text{m}$. The duration of the passivation step was increased to reduce the undercut.

Sample 3 also showed a large undercut ($15.1 \mu\text{m}$ undercut). This is still larger than what was expected, so the duration of the passivation step was increased, to the amount where an overpolymerization of the sample was expected. This was done to create a positive profile which could then be reduced.

The difference in undercut between sample 2 and 3 is contributed to the higher number of cycles, see table 2.1. Figure 3.2 show a SEM picture of sample 3 taken from above. The light areas are the masking layers without silicon underneath, the grey area in-between is the bottom of the groove. It shows that the amount of undercut is $15.14 \mu\text{m}$.

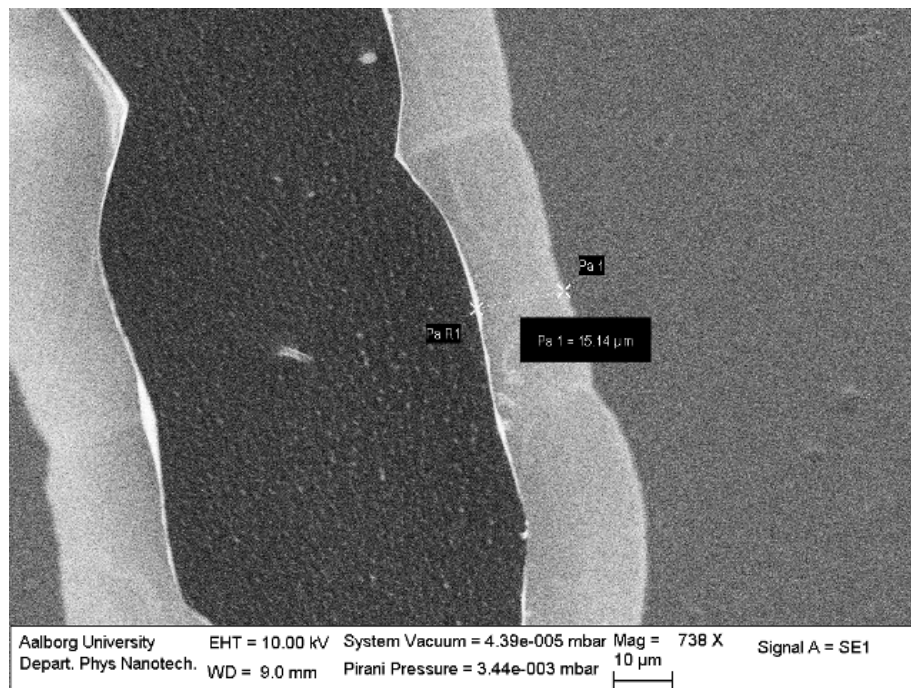


Figure 3.2: This figure show sample 3 as seen from above. The light areas are the masking layers without silicon underneath, the grey area in-between is the bottom of the groove. It shows that the amount of undercut is $15.14 \mu\text{m}$.

Sample 4 also showed a smaller undercut, than sample 2 and 3 had shown, but still larger than expected. The amount of undercut was in the range of around $5 \mu\text{m}$. However the etch depth was only $15.5 \mu\text{m}$ and even though the undercut was less, the ratio between the depth and the undercut was still large. A picture of sample 4 can be seen in figure 3.3. It shows a portion of the linear structure, which was used during the second optimization round.

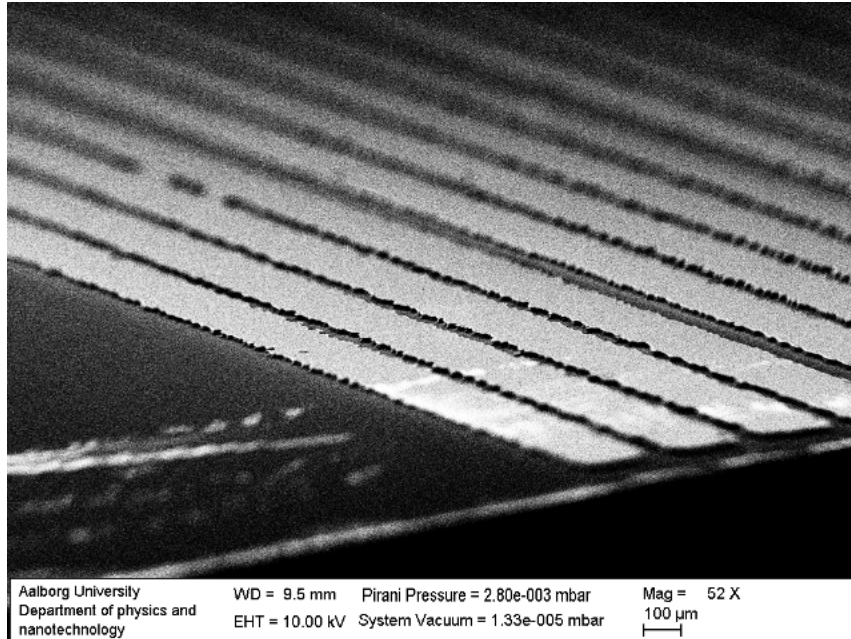


Figure 3.3: This figure shows a SEM picture of sample 4, tilted at an angle of approximately 60 deg . It show some of the structure used for the second optimization round. The light stripes are areas coated with Cr.

Based on the amount of undercut, the attempt of overpolymerization of the structure was unsuccessful. The bias voltage² was suspected to have an influence on the anisotropy, since it changes the directionality of the impending ions. The articles made by Wu et al. [12], Ayón et al. [16], and Chen et al. [28] were consulted, to review the parameters used during the etching and passivation step. The bias settings they used had a general tendency, were a "low" bias for the passivation step and a "high" bias for the etching step, was used. In an attempt to increase the bias during the etching step and lower the bias during the passivation step, a series of test were carried out on the RIE system. This was done to determine the connection between the bias, RF power and pressure. These results can be seen in figure 3.7 and 3.6. Before the results, found during the bias test, were implemented, the thickness of the masking material was increased to decrease the bending of the masking material layer, as can be seen in figure 3.4 and 3.5. These pictures show the masking material that bends around the structure. Trying to avoid this, the thickness of the masking material was increased to 20 nm .

²The bias voltage will in the result and the discussion section be referred to as either the bias voltage or just the bias.

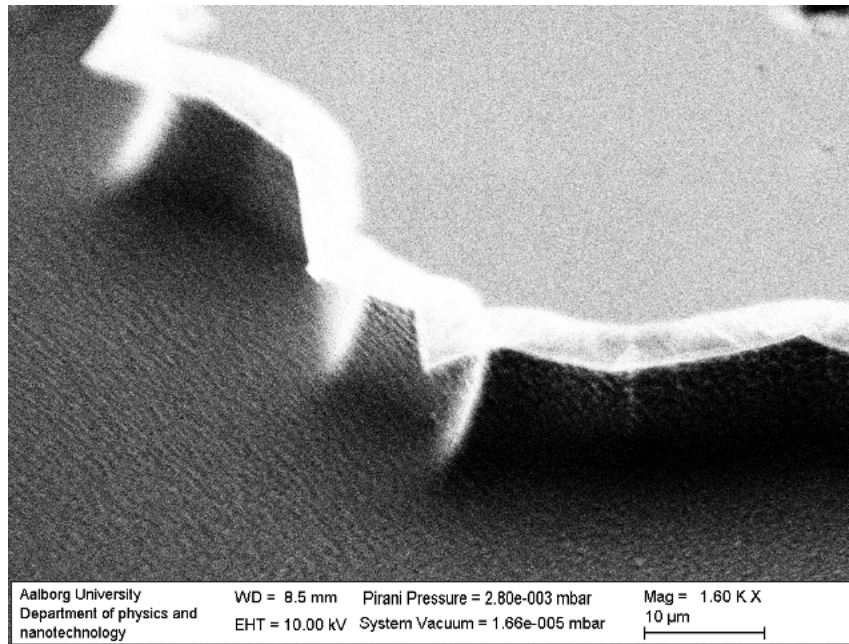


Figure 3.4: This figure shows a SEM picture of sample 4, tilted at an angle of approximately 70 deg. It shows the sidewall which has a large undercut.

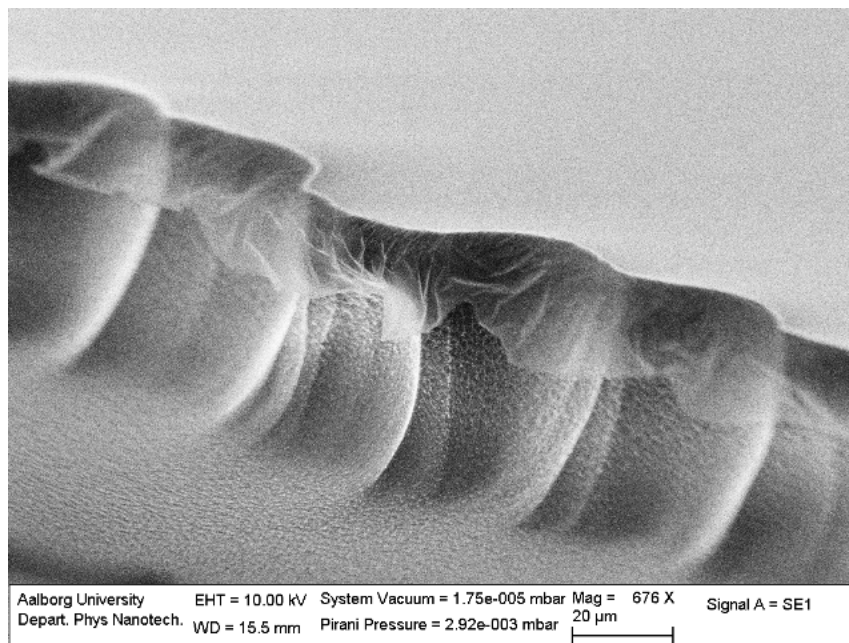


Figure 3.5: This figure shows a SEM picture of sample 3, tilted at an angle of approximately 80 deg. It shows the sidewall and the thin material dangling from the top is the masking material.

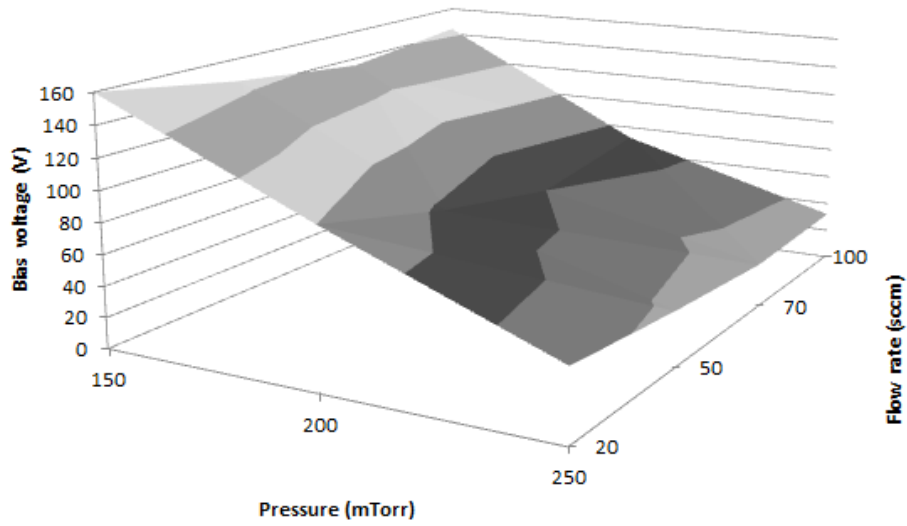


Figure 3.6: Bias voltage as a function of pressure and flow rate for C_3F_8 plasma. The RF power was kept at 250 W at all times.

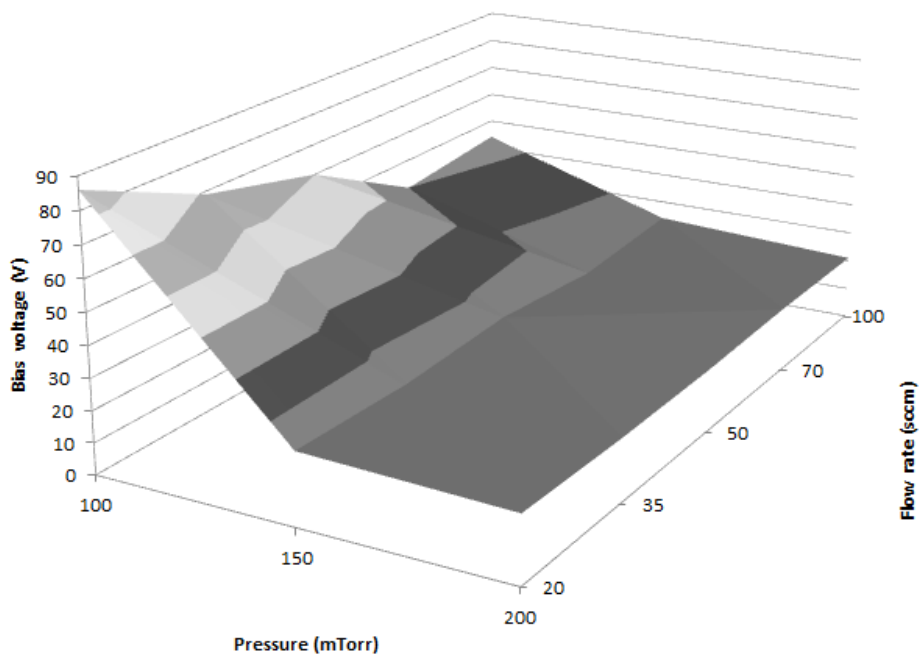


Figure 3.7: Bias voltage as a function of pressure and flow rate for SF_6 plasma. The RF power was kept at 300 W at all times.

Sample 5 was the first sample to use the thicker masking material, therefore the same process parameters were used, as during the etching of sample 3. During the process the plasma was unstable and flickered without reason, therefore the process was aborted and the entire process was tried again on sample 6.

Sample 6 showed a significant drop in etch rate, compared to sample 3. The drop in etch rate was suspected to be connected with the plasma error of sample 5, or perhaps the chamber needed cleaning based on the experiences made by Jansen et al., [15]. The chamber was cleaned by exposing it to an oxygen plasma for 8 hours, the cleaning of the chamber is discussed in section 3.2.11.

Sample 7 was etched using the same process parameters, to investigate the effect of the cleaning. However the drop in etch rate persisted and no literature could give a clear explanation behind this drop in etch rate. Due to this, the drop in etch rate was deemed as a low priority, versus that of getting the Bosch process to work, and the results from the bias test were implemented on sample 8.

As a result of the bias test, sample 8 showed an increase in anisotropy by an increase in etching depth - undercut ratio, see figure 3.8 and 3.9. The two figures show sample 8 from above and from the side, respectively. Figure 3.8 show the sample from above, where the white stripe is the masking material without silicon underneath. Figure 3.9 show the sidewall of sample 8, the white area is the masking material and the vertical grey area is the sidewall. This clearly show that the structure has suffered some undercut. However the undercut was still larger than required.

Inside the reactor chamber of the RIE system was a big wafer. The wafer had, in previous experiments, shown to have a stabilizing effect on the plasma. In this experiment it was suspected to inhibit the promotion of the protective passivation layer, therefore it was removed in an attempt to enhance the anisotropy.

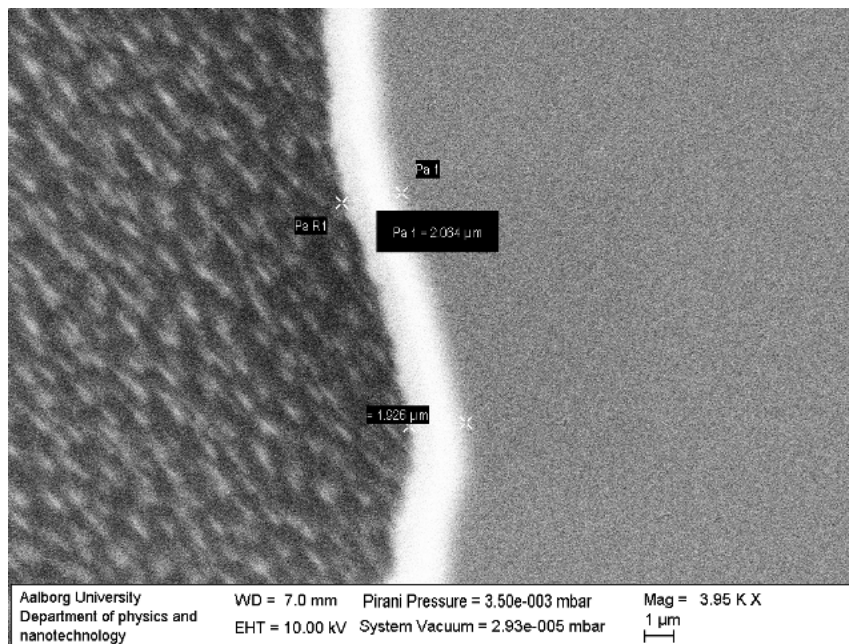


Figure 3.8: This figure shows sample 8 imaged from the top at 0 deg inclination. It show that the amount of undercut is around 2 μm.

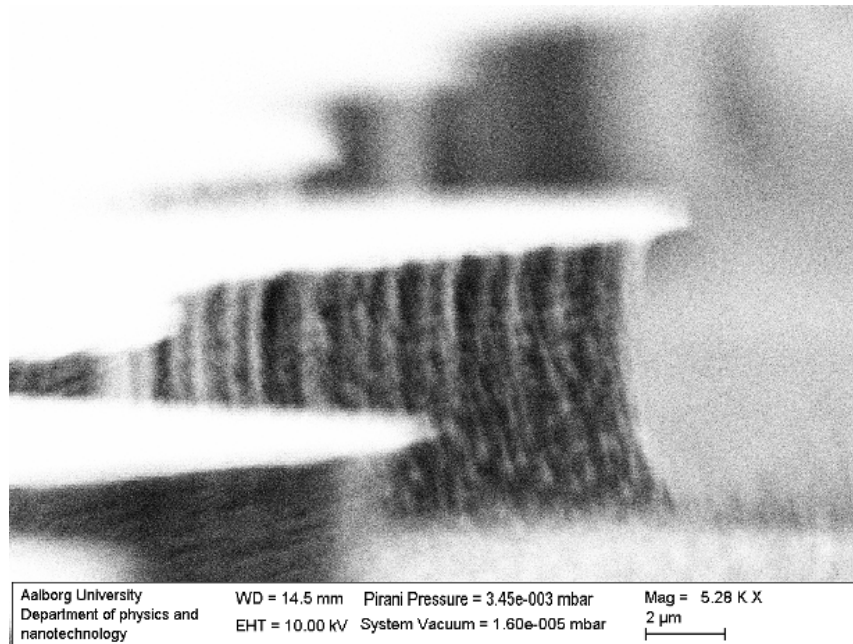


Figure 3.9: This figure show a picture the sidewall of sample 8. The white area is the masking material and the vertical grey area is the sidewall. The picture is taken at an inclination of ~ 80 deg.

Prior to sample 9, the deposition rate of the passivation layer was measured, to make sure the polymer formation was dominant. The deposition rate of C_3F_8 was 16 nm/min, with the same passivation process parameters as sample 9.

Sample 9 showed a "large" increase in etch rate but still a large undercut ($2.5 \mu\text{m}$) was observed. To reduce this undercut, the duration of the passivation step was increased, to deposit a thicker layer of the passivation layer.

Sample 10 showed a significant increase in the vertical etching and a clear reduction of the amount of undercut, see figure 3.10. The figure shows a SEM picture of the structure, tilted at approximately 80 degrees angle. It is clear that the amount of undercut is decreased significantly, if compared to any of the previously samples. However a profile with a vertical sidewall is desired. In-order to achieve this, the duration of the passivation step was increased.

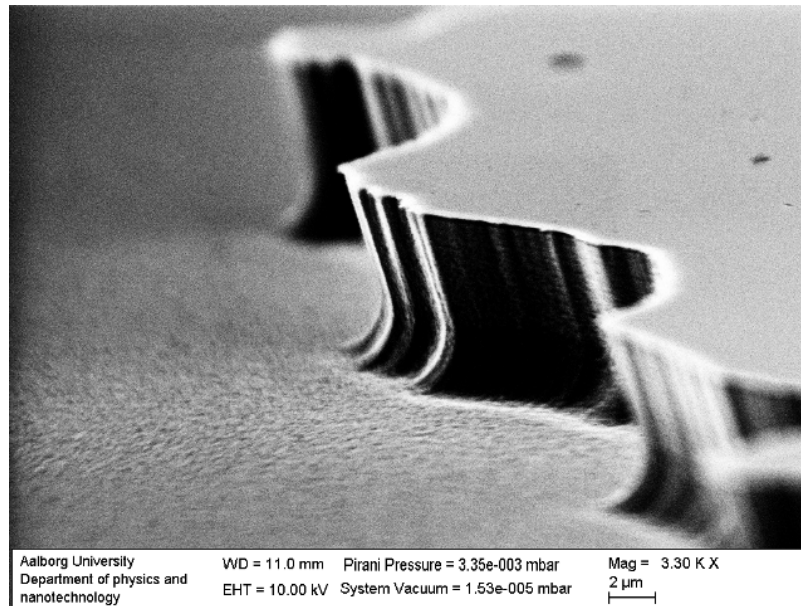


Figure 3.10: This figure show a SEM picture of sample 10 tilted at approximately 80 degrees angle. The two surfaces that are parallel are the masking material and the bottom of the trench.

Sample 11 was the first sample to exhibit the characteristic sidewall scallops, of the Bosch process. This is shown in figure 3.11 where the white stripes on the sidewall are the peaks of the scalloped surface. The sidewall was not vertical, therefore the duration of the passivation step was increased even further.

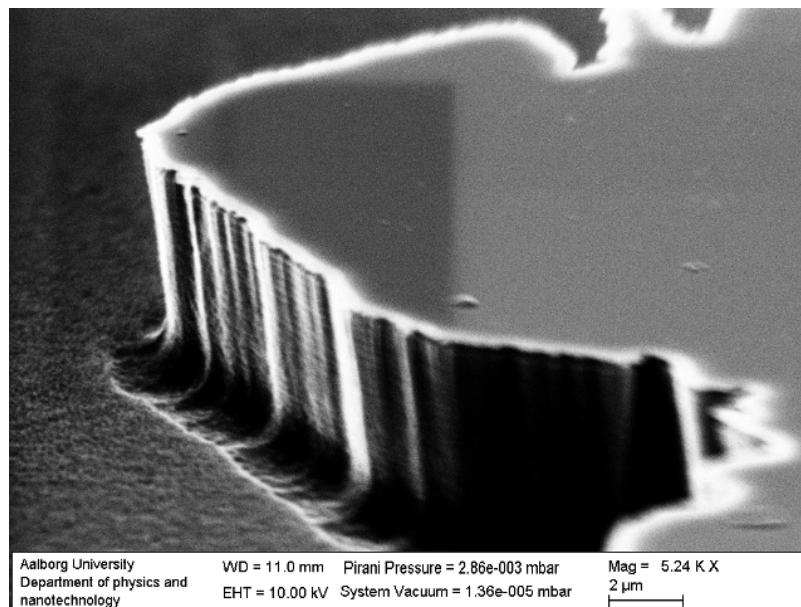


Figure 3.11: A SEM picture of sample 11 tilted at approximately 70 degrees angle. The white stripes on the sidewall are the peaks of the scalloped surface.

Sample 12 shows clearer signs of sidewall scalloping. This is clearly visible in figure 3.12, which shows a scalloped sidewall and a small undercut at the top of the structure, these are characteristic for the Bosch process. Figure 3.13 shows a close-up of the top of a sidewall. This shows an undercut of 307 nm. The linear structure exhibited the characteristic trademarks that were required as a basis to expand the process. It exhibited the straight profile, small undercut, small scalloping, and the capability to vary and change these as desired. Based upon this, the choice was made to expand the experiments, to a new type of structure. This concluded the second optimization round.

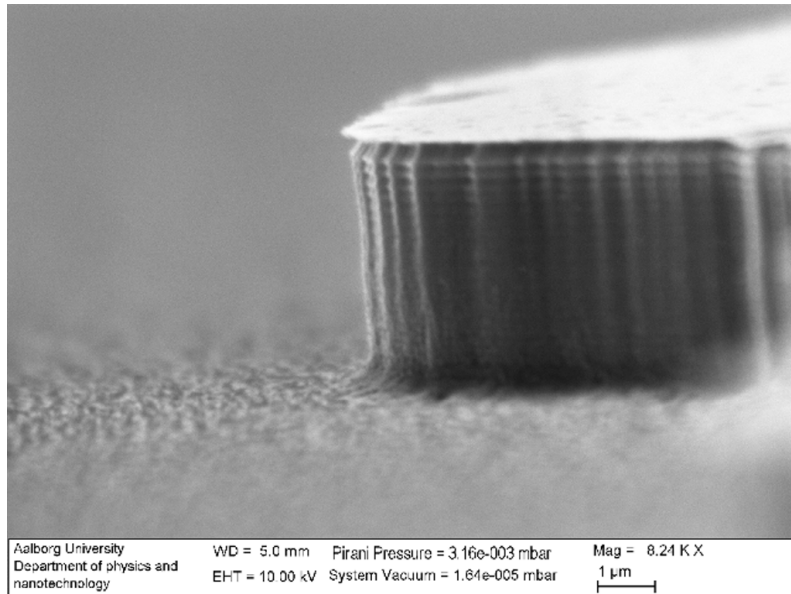


Figure 3.12: This figure shows a SEM picture of sample 12 which has an undercut, and a clear scalloped sidewall.

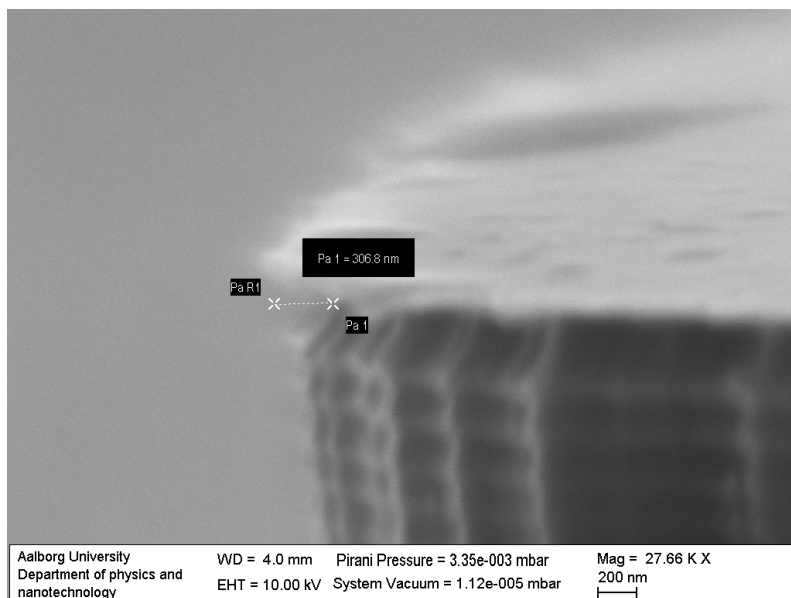


Figure 3.13: This figure shows a SEM picture of sample 12. The undercut after 21 cycles is only 307 nm.

3.1.3 Third optimization round

Now that the Bosch process had been proven to work on a large structure, a new smaller structure was needed to better fit the parameters of the GRIN-lens structure and make them comparable. The comb structure was developed, it was made on the premise that the structure needed to: be linear, display an array of trench widths, have the ability to be viewed from different angle, and display the trenches without having to physically break the sample. The fact that the sample does not have to be broken has a clear advantage, since it can be examined during and after it is being processed without changing the parameters. This is not the case for several articles, e.g Ayón et al. [16] and Vyvoda et al. [29] both breaks the sample afterwards and have to start over, if the process is faulty or needs a longer exposure time.

The first draft of the comb structure can be seen in figure 3.14. The structure was later redesigned and ended up looking like figure 2.2. This was done due to the fact that it was impossible to look at the trenches, if the sample was tilted more than approximately 75 degrees.

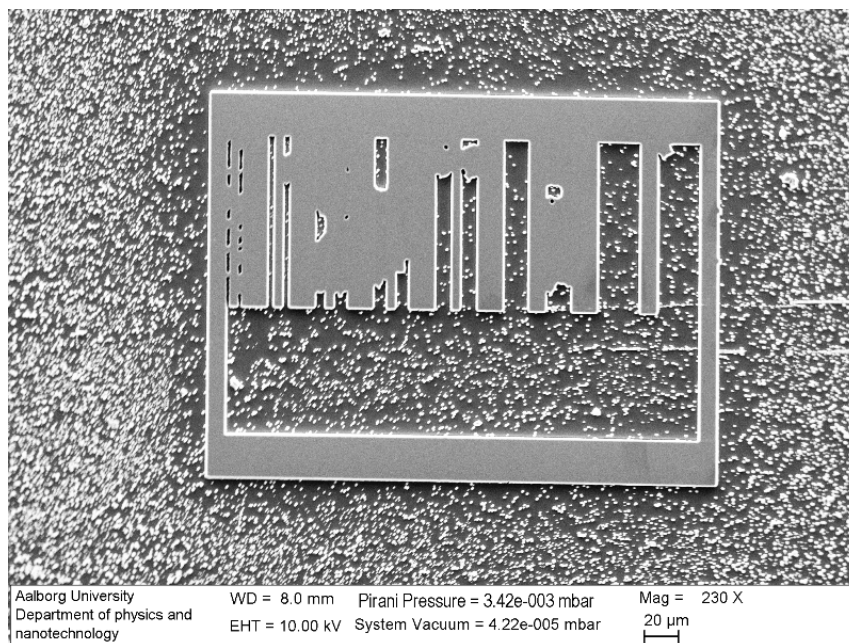


Figure 3.14: This figure shows a SEM picture of sample 13 taken at an inclination of 0 deg. It shows the entire comb structure on sample 13. The structure shows some lift-off related issues due to the fact that almost non of the trenches are clear of masking material.

Sample 13 exhibits what is called a positive profile and some problems regarding the formation of micrograss, this can be seen in figure 3.15. The profile angle was measured to be 4.2° . Figure 3.14 shows that sample 13 exhibited some problems regarding the lift-off procedure. This is visualised by the lack of trenches in the structure. Due to this lift-off related problem, the thickness of the masking material on sample 14 was decreased to 15 nm. The solution to the positive profile was solved by, decreasing the duration of the passivation step. The formation of micrograss was not investigated since it did not occur inside the trenches in large formations, and due to the fact that it was not considered a critical parameter

by Ayón et al. [16] and Wu et al. [12]. The micrograss formation and influence will be discussed in section 3.2.7.

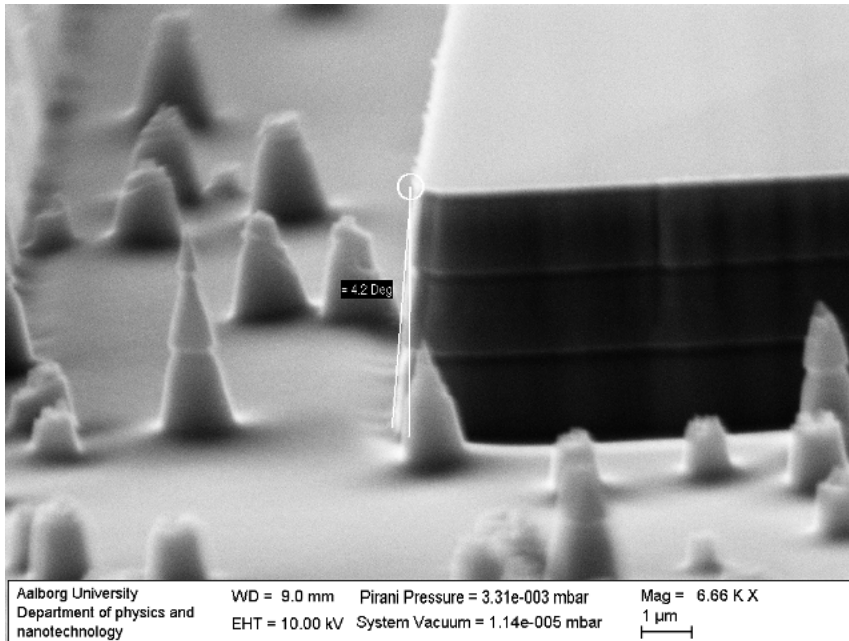


Figure 3.15: This figure shows a SEM picture of sample 13 tilted at approximately 80 degrees angle. The profile angle have been measured using the SEM software.

Sample 14 showed a structure with a vertical profile. The lift-off related problem had been resolved to some extent. The trenches had been almost cleared, since the narrow trenches still had some issues, as can be seen in figure 3.16. This figure shows an overview of the entire structure on sample 14. The trenches which are not fully cleared are the 2 μ m and 4 μ m wide trenches. The micrograss related problem had decreased a lot and the change in the design gave a better opportunity to investigate the individual trenches. The dependence between the duration of the passivation step and sidewall profile was investigated by decreasing the duration of the passivation step.

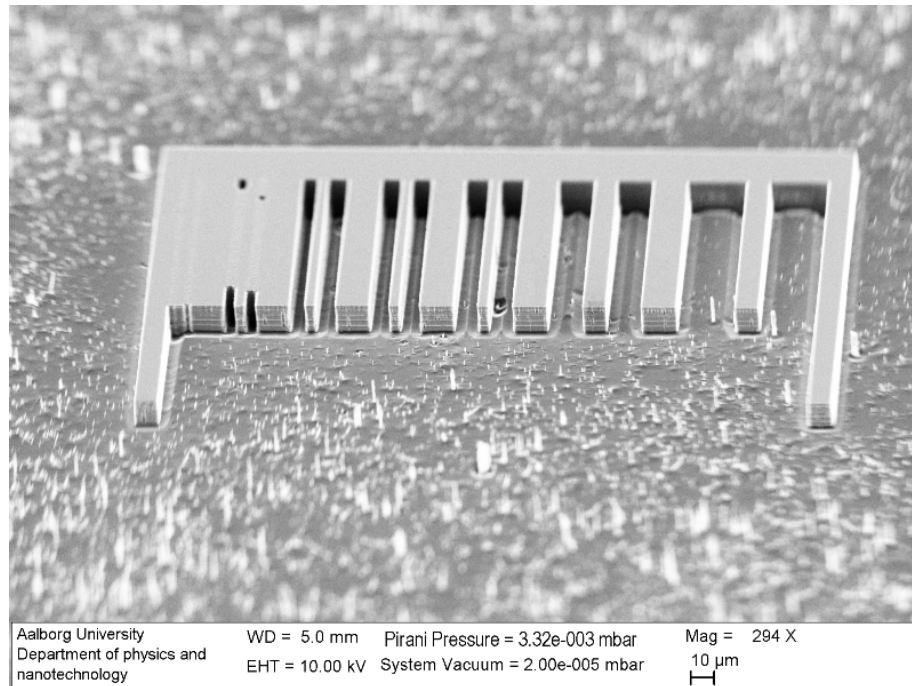


Figure 3.16: This figure shows a SEM picture of sample 14. It shows the entire comb structure. The small white needles are micrograss.

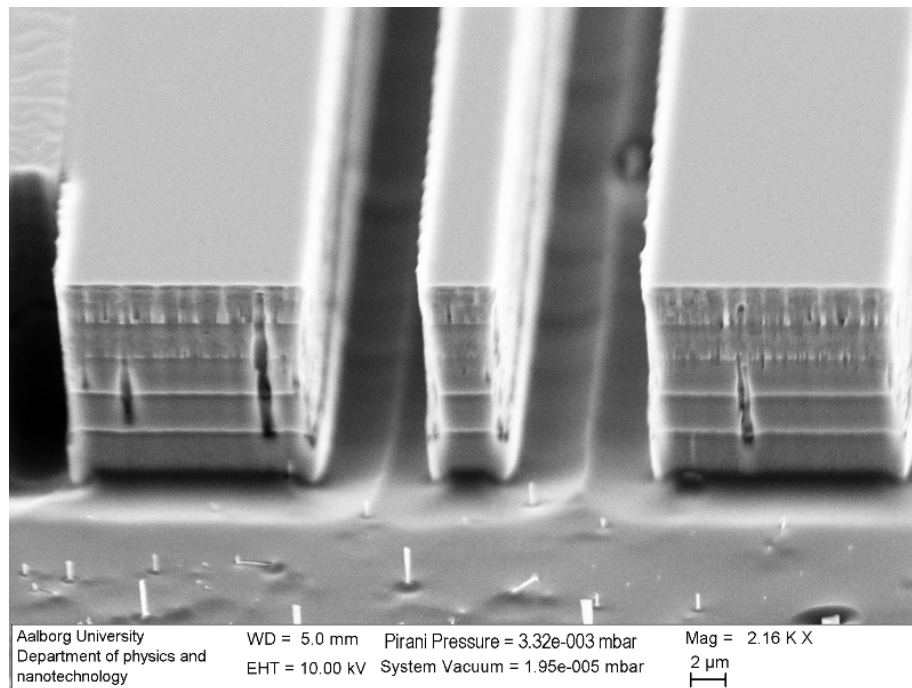


Figure 3.17: This figure shows a SEM picture of sample 14. It shows a close-up of the 6 μ m wide trench. A microtrench can be seen running along the sidewalls.

Sample 15 showed a slightly negative profile, some micrograss formations, and the lift-off related problem was still unresolved. The lift-off related problem was still there regarding the narrow trenches ($2\text{-}4\ \mu\text{m}$). In an attempt to achieve lift-off on the smaller features the sample had been heated in an acetone bath and then exposed to the ultrasonic bath. However this did not solve the problem. The problem was solved in the case of sample 16, where a new 3% PMMA solution was mixed and a can be seen in figure 16, this solved the problem, even though the thickness of the masking material was actually increased.

Sample 15 had a roughening band, which can be seen in figure 3.19. The roughening band is the term used for the increase in surface roughness, starting at the top of the sidewall and ending a little below the middle. This roughening band was also experienced on sample 14, see figure 3.17, and will be discussed in section 3.2.8. Sample 15 also shows signs of microtrenches. This can be seen as the trench on both sides of the sidewall, stretching from the sidewall, to the peak in the bottom of the trench, as seen in figure 3.19. Some of the other microtrenches in other trenches, on the same sample, can be seen in figure 3.22, 3.24, and 3.23. The microtrench formation is visible on all the samples, using the comb structure and will be discussed in section 3.2.4.

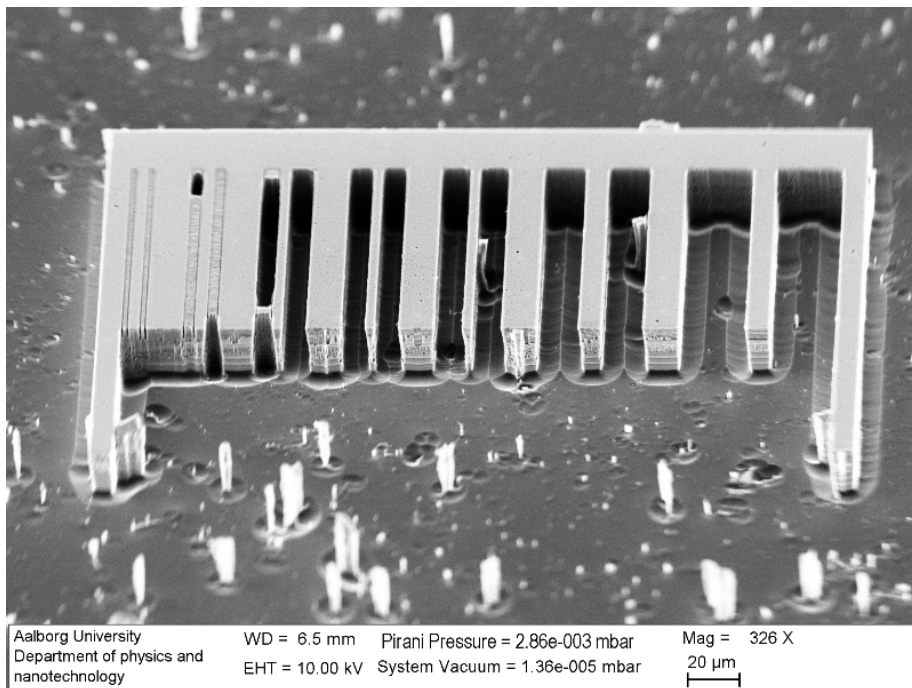


Figure 3.18: This figure shows a SEM picture of the comb structure on sample 15. The pillars not part of the structure are micrograss formations.

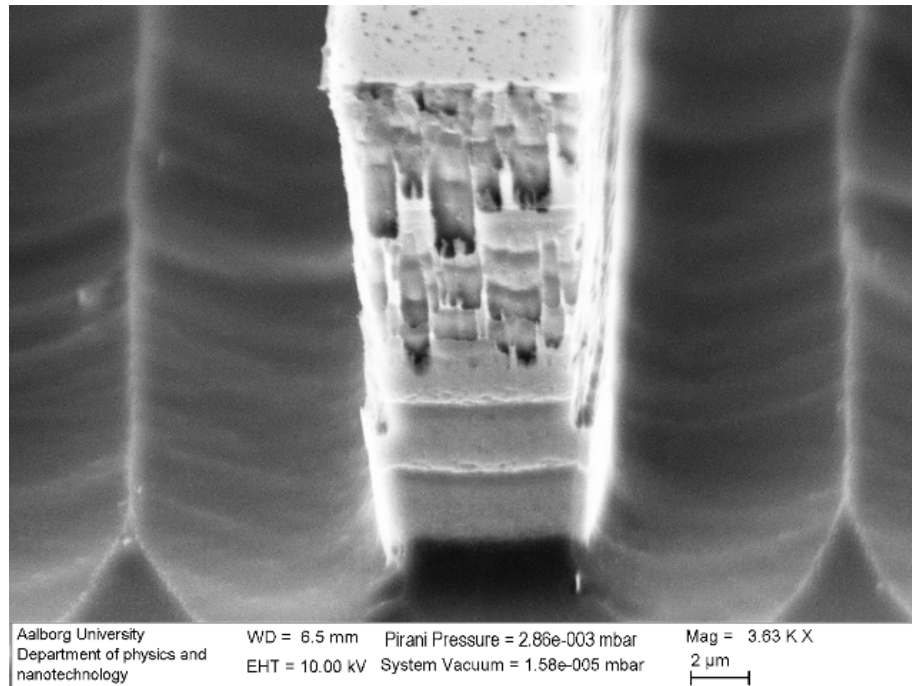


Figure 3.19: This figure show sample 15. A roughening band can clearly be seen on the sidewall. This roughening band is approximately $13.5 \mu\text{m}$ thick. The figure also shows two microtrenches, one on each side of the sidewall.

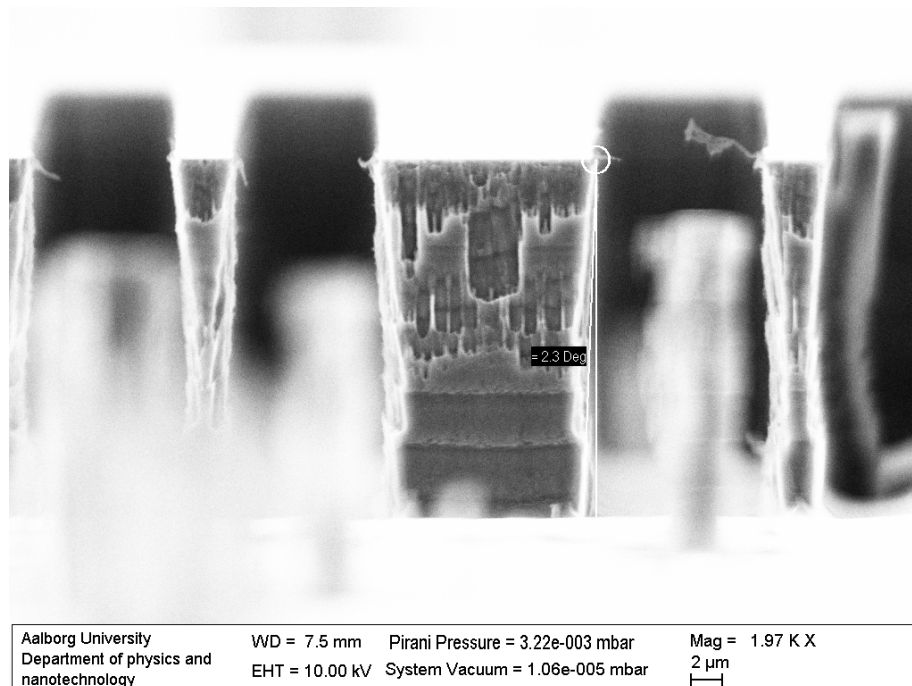


Figure 3.20: This figure shows a SEM picture of sample 15. The profile angle have been measured with the SEM software.

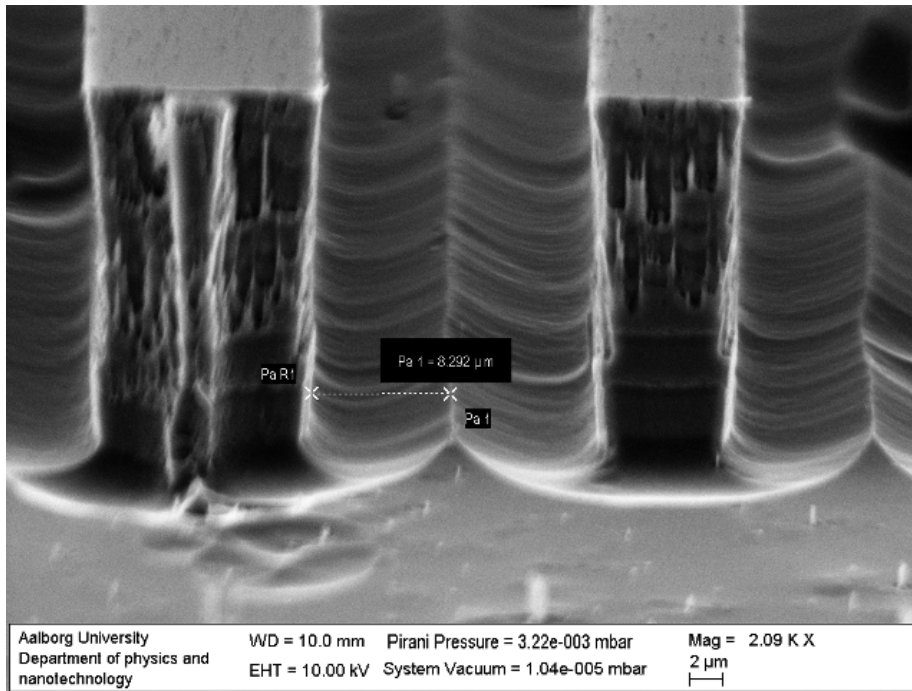


Figure 3.21: This figure shows a SEM picture of the bottom trench of sample 15. The trench in the middle should be 15 μm wide. The microtrench in the 15 μm wide trench is 8.3 μm wide.

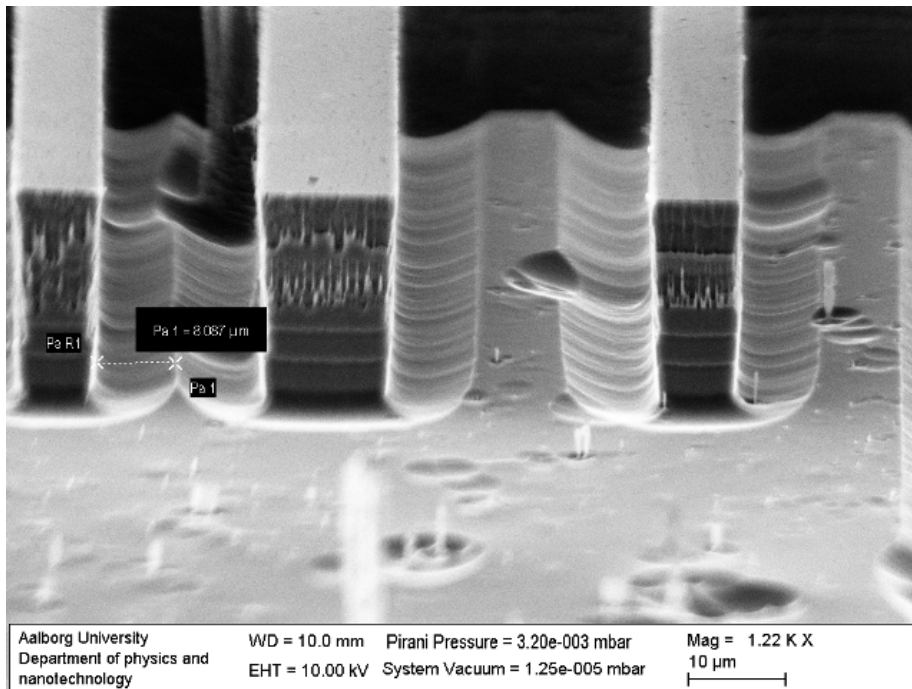


Figure 3.22: This figure shows the bottom trench of sample 15. Where the first trench from the left should be 15 μm wide and the next should be 25 μm wide. The microtrench in the 15 μm wide trench is 8.07 μm wide.

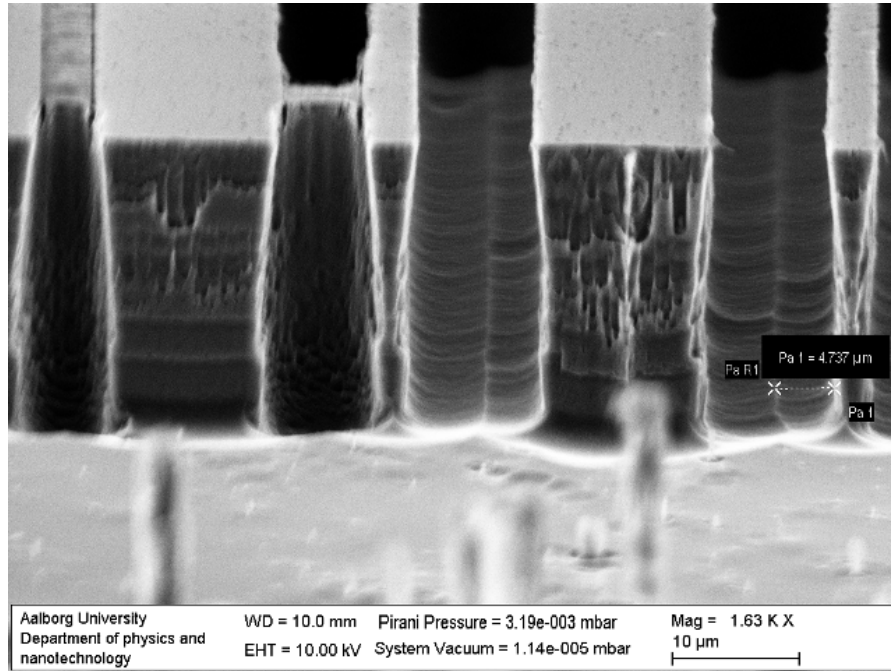


Figure 3.23: This figure show the bottom trench of sample 15. Where the first trench from the left should be 4 μm wide and the two next should be 6 μm wide, and the far right trench should be 8 μm wide. The microtrench in the 8 μm wide trench is 4.74 μm wide.

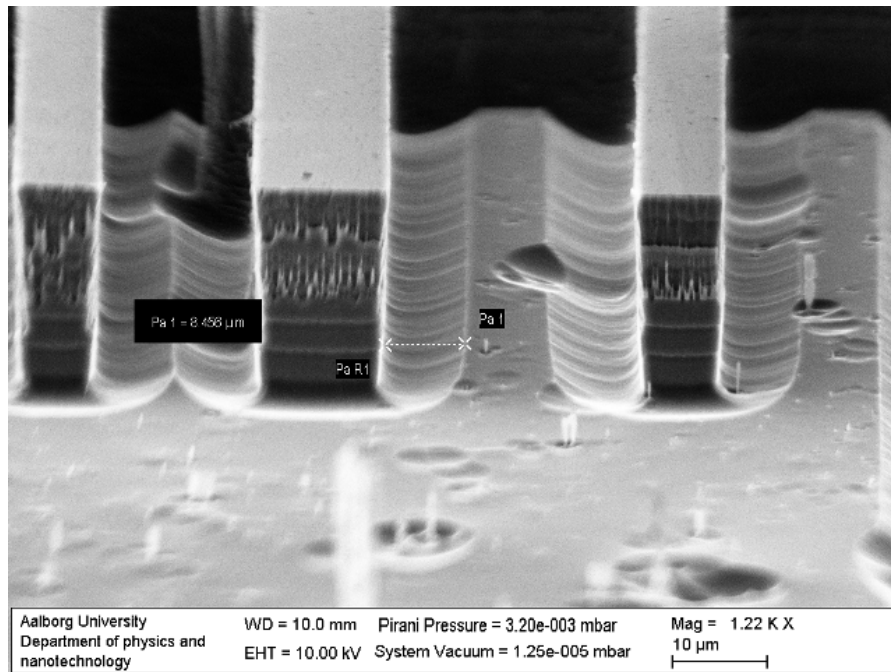


Figure 3.24: This figure show the bottom trench of sample 15. Where the first trench from the left should be 15 μm wide and the next should is 25 μm wide. The microtrench in the 25 μm wide trench is 8.46 μm wide.

The theoretical structure made by Brincker and Karlsen, [1] was based on an a structure with an AR of 40. This made the current AR of ~ 10 insufficient, and the etch needed to be deeper. Sample 15 showed a negative profile, and was therefore not used in the attempt to achieve a higher AR, since a deeper etch would increase the chance of the structure being destroyed, due to a breaking of the sidewalls. Based on this the process parameters of sample 14 was used. However as can be seen on figure 3.25 the sample was greatly deteriorated after approximately 336 cycles. It is clear that the sample was deteriorated due to a lack of masking material, since the entire structure had been reduced in height. The solution to this problem, was to increase the thickness of the masking material to 33 nm.

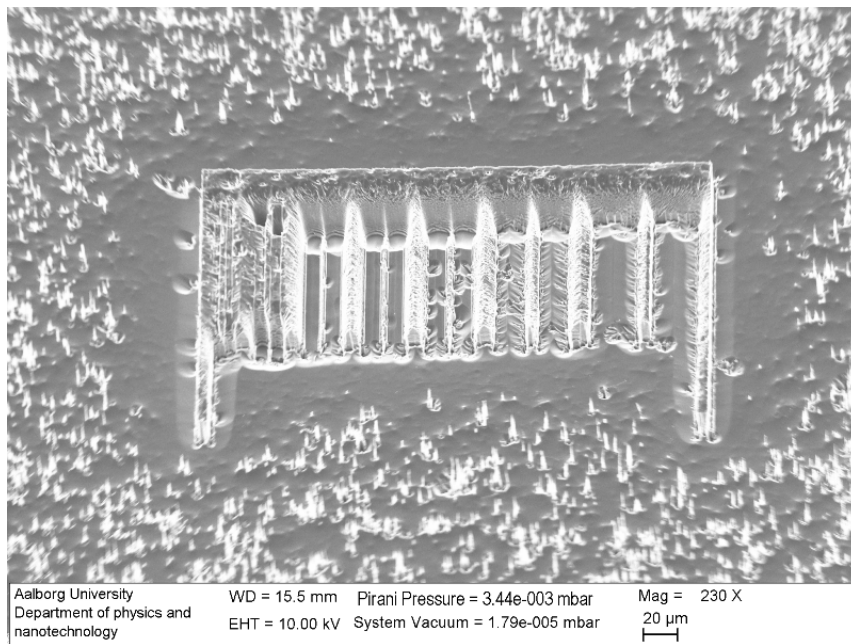


Figure 3.25: This figure shows the deteriorated structure of sample 14.

Sample 16 after 105 cycles, as can be seen in figure 3.26, exhibited the problems described earlier, such as formation of microtrenches, formation of micrograss, and low etch rate. However the lift-off related problem had been solved by using a new 3% PMMA solution. The roughening band seen in figure 3.18 had been reduced greatly. The solving of the lift-off related problem had caused a new problem involving the smaller features, where a clear etch rate non-uniformity and a bowing of the trench can clearly be seen in figure 3.26. The figure show an overview of the entire comb structure on sample 16. The micrograss formations and the microtrench formations are clearly visible. As can be seen in figure 3.27, which is a closeup of the sidewall on sample 16, the sample does still show the characteristic trademarks of the Bosch process. It shows a reduced amount of scalloping, compared to sample 12, and a small undercut right beneath the masking layer. A darker vertical line in the middle of the picture can be observed and will be discussed in section 3.2.6. This was results from the structure after 105 cycles.

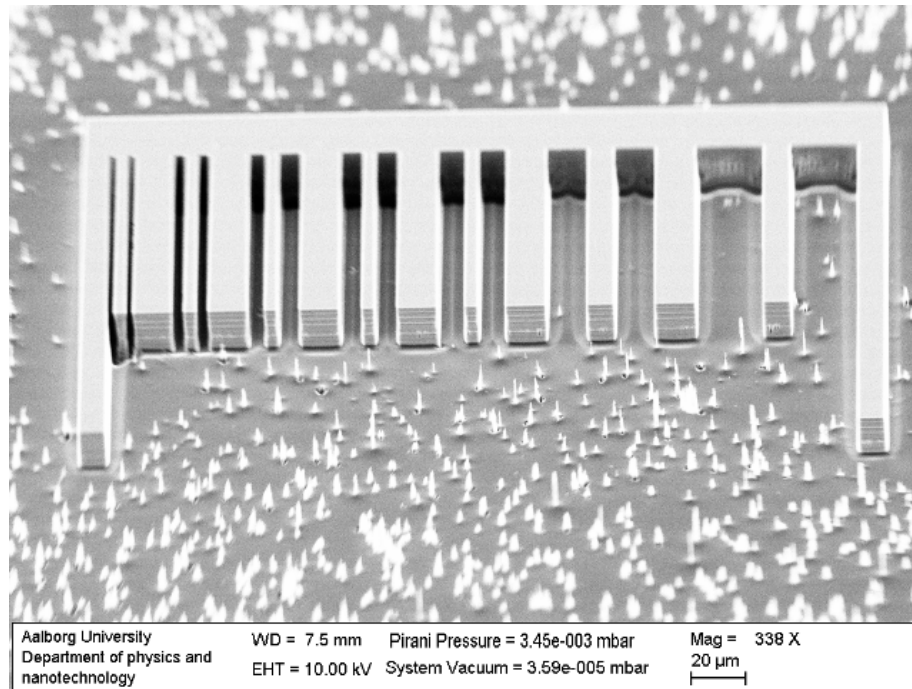


Figure 3.26: This figure show the entire comb structure on sample 16. A microtrench can clearly be seen in the individual trenches. A difference between the size of the microtrenches can be seen. The white needle like shapes, on the bottom of the sample, is the formation of micrograss.

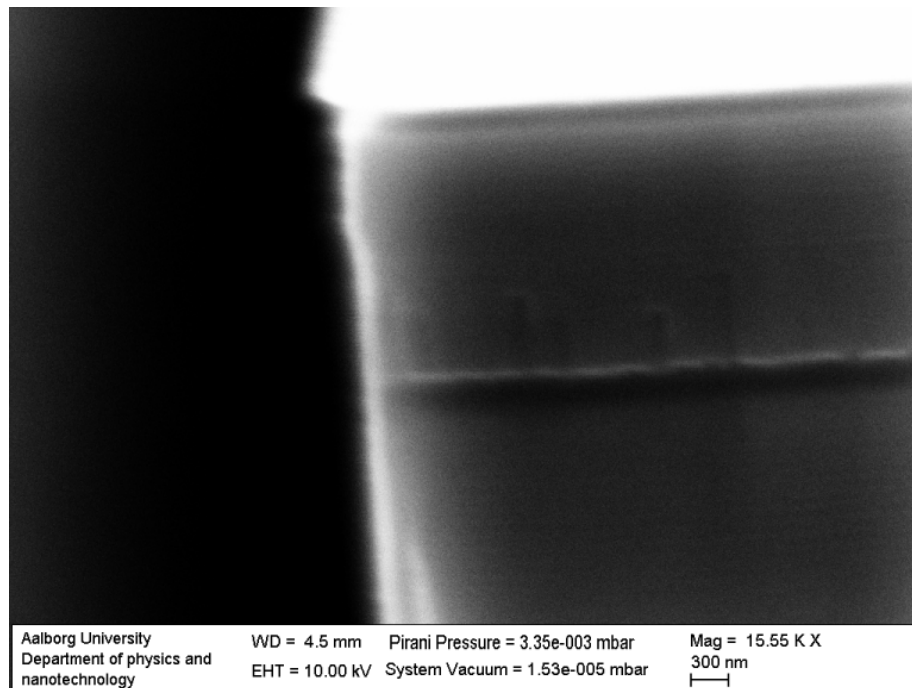


Figure 3.27: This figure show a SEM picture of the sidewall of sample 16 which has a "large" undercut of the first step and a scalloped sidewall.

Figure 3.28 show sample 16 after 399 cycles. It clearly shows some heavy deterioration of the entire structure. The thinner walls in the smaller trenches show signs of heavy deterioration, as opposed to the walls in the larger trenches. It is clear that the etch rate is non-uniform across the structure, since the smaller trenches show a higher etch rate than the larger structures. The smaller trenches also exhibit signs of bowing.

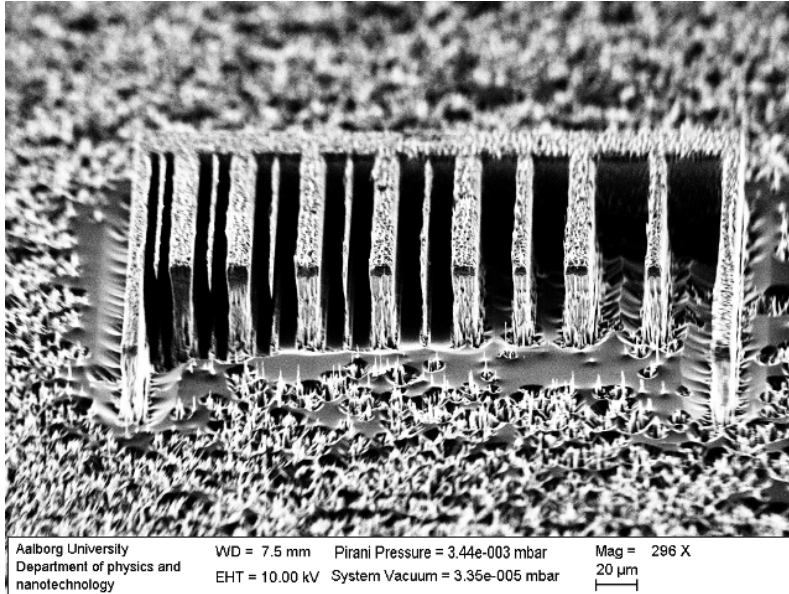


Figure 3.28: This figure shows a SEM picture of sample 16. The picture is taken after approximately 400 cycles. It is easy to see how the structure is deteriorated.

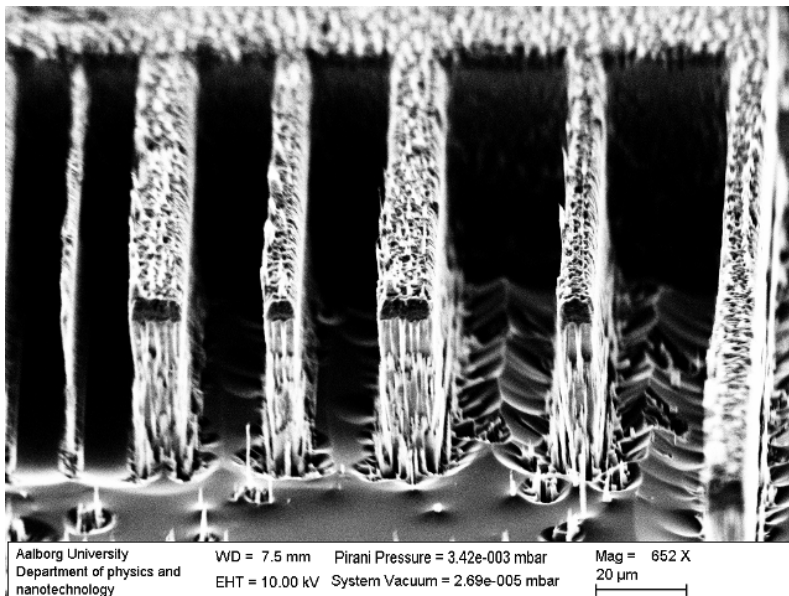


Figure 3.29: This figure shows a SEM picture of sample 16. The picture is taken after approximately 400 cycles and shows the six widest trenches in the comb structure.

Figure 3.29 show a SEM picture of sample 16. It is a closer look at the wider trenches, seen on figure 3.28. It is clear how the structure has deteriorated, the sidewall roughness has increased, micrograss has been created on the top of the structure, and the bottom of the trenches are not as even as on figure 3.26. To solve the deterioration problem the thickness of the masking material was increased even further to a thickness of 67 nm.

As can be seen in figure 3.30 and 3.31 the structure of sample 17 show heavy signs of micrograss formation. The micrograss inside the trench of sample 17 is somewhat different from the micrograss outside the trench, but also different from the micrograss seen in figure 3.18. The micrograss formation will be discussed in section 3.2.7.

The structure exhibited a small undercut which can be seen in figure 3.32. This figure is a close-up of the top of a sidewall of sample 17. It shows an undercut of 337 nm.

Due to this strong increase in micrograss formation on sample 17 the process parameters for the lens structure was chosen to be those of sample 16.

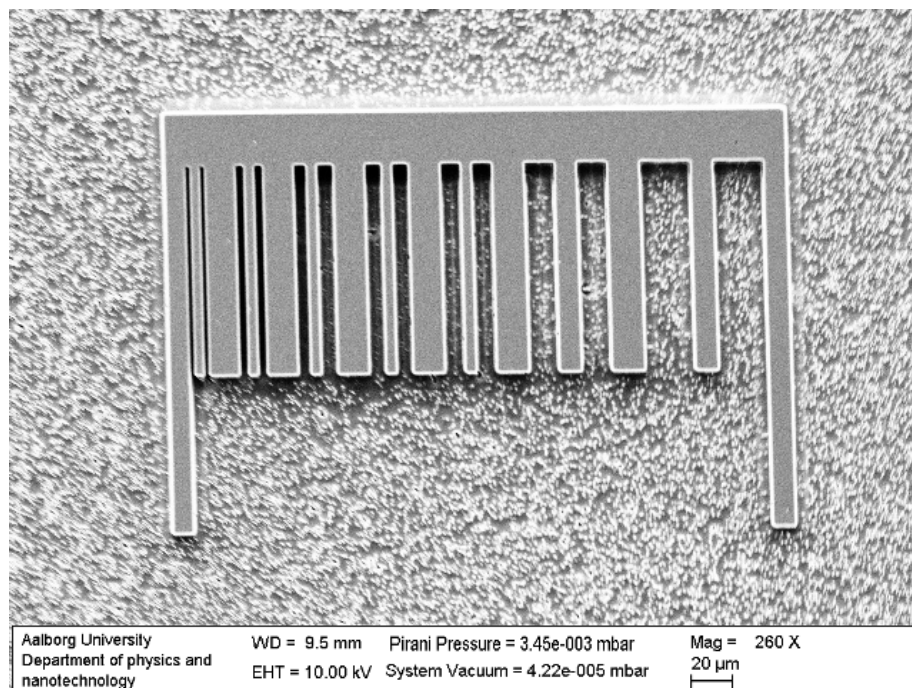


Figure 3.30: This figure shows a SEM picture of sample 17 as seen from above. It shows the entire comb structure. The white spots are micrograss.

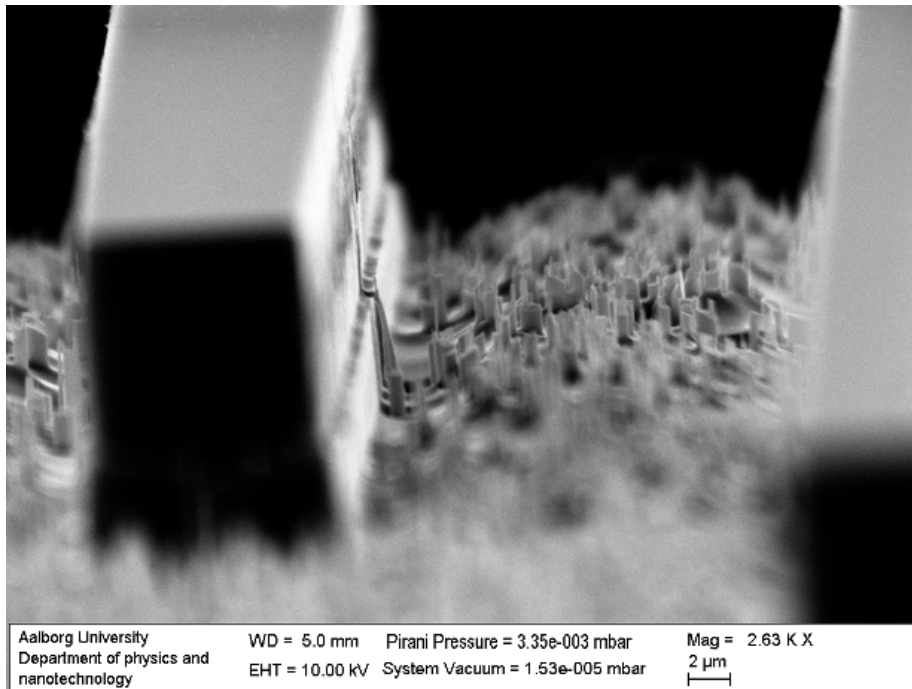


Figure 3.31: This figure shows a SEM picture of sample 17. A formation of micrograss at the bottom trench is clearly seen. This picture is of the widest trench.

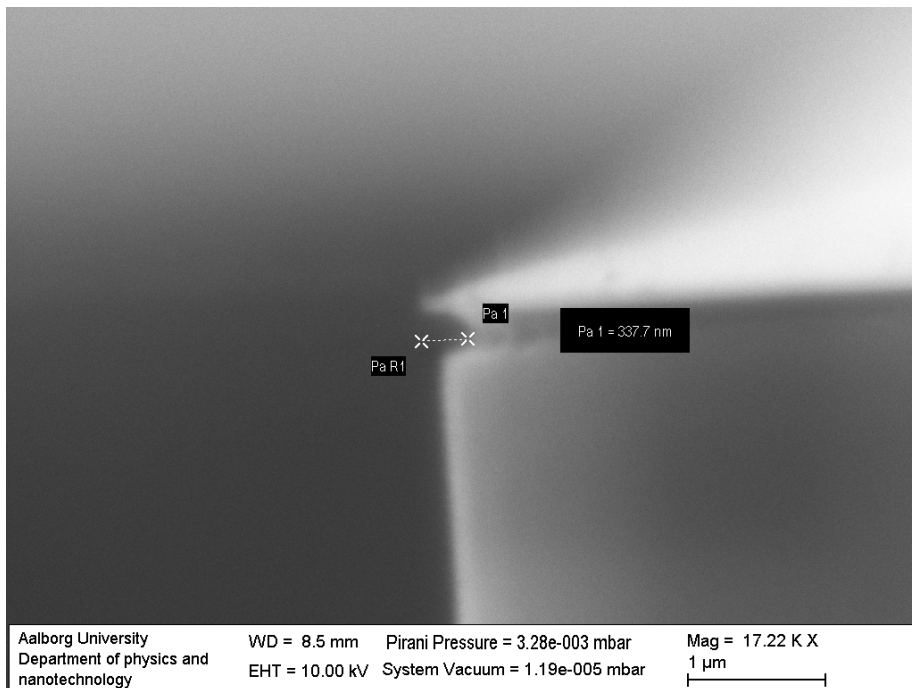


Figure 3.32: This figure shows a SEM picture of sample 17. It shows that the undercut of sample 17 after 84 cycles is only 337 nm.

3.1.4 Fourth optimization round

The fourth optimization round was an attempt to use the experience gained during the other optimization rounds, and apply it during the fabrication of the lens structure, based on the design by Brincker and Karlsen, [1].

The lens structure created by Brincker and Karlsen, [1] has a diameter of $700\ \mu\text{m}$. The problem arises when trying to expose the entire lens structure in one take. This could not be done due to problems regarding the write field of the Zeiss 1540 XB. Due to this only part of the lens structure was developed. This resulted in an exposure and developing of the four inner rings, as seen in figure 3.33. The inner rings were developed to prove that the Bosch process is independent on the structure shape.

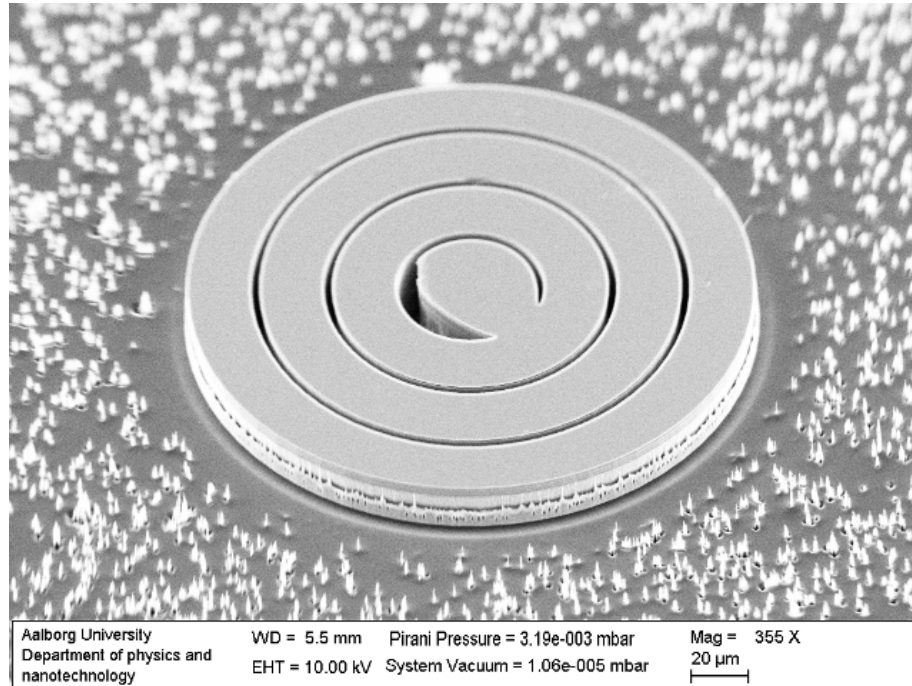


Figure 3.33: This figure show the entire fabricated lens structure, referred to as lens 1. It is only the four inner rings and the structure has a diameter of $200\ \mu\text{m}$.

3.2 Discussion

3.2.1 Isotropic Etching

Sample 1–9 showed clear signs of isotropic etching characteristic with limited passivation, see figure 3.9 and figure 3.4. It is clear that the sidewall is not protected enough and the undercut is more prominent than the undercut on e.g. figure 3.10. The isotropic etching is less in sample 8, as can be seen in figure 3.9. This isotropic etching of silicon concurs with the theory, which describes the etching of silicon using SF_6 as isotropic by nature.

The reason behind the missing passivation layer is contributed to the bias voltage. With the bias voltage for the first 7 samples being 170 V and the F/C ratio being 2,6 for C_3F_8 , this puts the polymer formation in the etching regime, according to figure 1.11. Even though the duration of the passivation step for sample 4, was high enough to introduce the desired profile, the passivation step would etch instead of producing the protective film, hence leaving the sidewall unprotected. It was not until the bias was lowered enough, that the polymer formation was promoted and the sidewalls were protected.

3.2.2 Etch Rate

The results clearly show a drop in etch rate, as the duration of the passivation step is increased, see figure 3.34. The main reasons for this drop in etch rate is subjected to an increase in passivation film thickness and an increase in overall cycle duration. A way to decrease the drop in etch rate, would be to increase the deposition rate of the passivation layer. The etch rate of 60 nm/min is slow compared to e.g Ayón et al. [16] who easily achieved etch rates between 2-3 $\mu\text{m}/\text{min}$. However they achieved this etch rate using an ICP which gives a higher plasma density. The RIE system, used in the project, used a capacitively coupled plasma which can supply as high a density as an ICP. According to the theory a higher plasma density increases the etch rate.

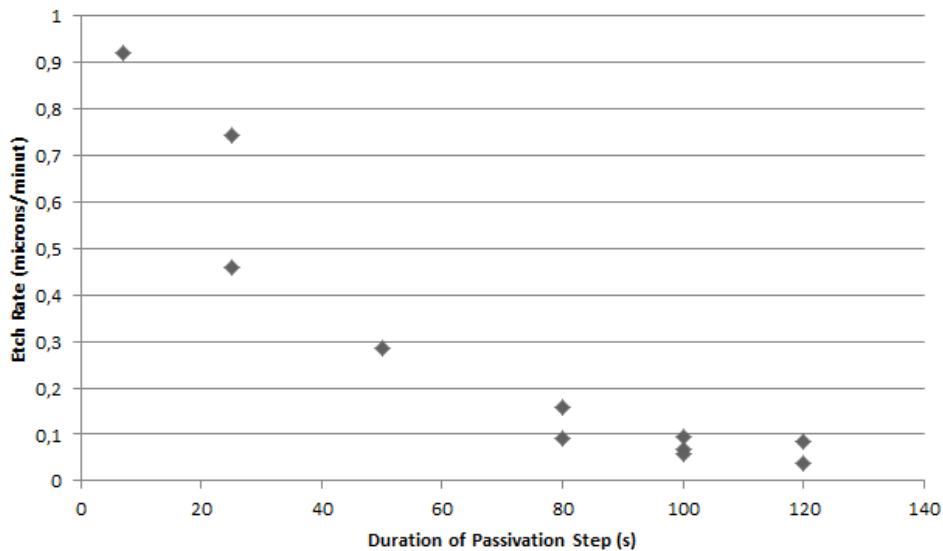


Figure 3.34: This graph shows the connection between etch rate and passivation time found in table 2.1.

The etch rate of Si using only the SF₆ gas was measured to investigate the etch rate without the influence of the passivation step. A clear relationship between RF power and etch rate was found, see figure 3.1. This neglects the influence of the masking material and the loading effect, but it shows the connection between etch rate, RF power and flow rate. It clearly show that an increase in RF power leads to an increase in etch rate no matter the flow rate. It also show that the etch rate is not independent on the flow rate since there is a noticeable difference when the RF power is above 400 W. However when the RF power is below 400 W, the etch rate is not nearly as dependant on the flow rate. This makes sense since the RF power is the dominant variable that controls the silicon etching rate, because an increase in RF power increases the degree of ionization of the plasma.

Ayón et al. [30] investigated the connection between etch rate, RF power and flow rate. They also stated that an increase in RF power and flow rate, will lead to an increase in etch rate. According to Ayón et al. [30] an increase in flow rate leads to an increase in etch rate, due to the removal of SiF₄ products, that would otherwise redeposit. They also stated that the etch rate increases with pressure.

Due to the programming of the RIE, there is a cycle overlap where one gas is pumped out and another is pumped in. This results in a longer duration of the etch and passivation steps than actually informed. The active cycle overlap does not only extend the etching time overlap but more importantly it reduces the flickering of the plasma, when switching between the two plasmas. This leads to a more stable plasma. The cycle overlap of the etching and passivation step can be removed, by placing an additional step that would empty the chamber between the two steps. This would remove the problem of the overlap, however it would increase the production time. According to Ayón et al. [16] the active cycle overlap is a good thing, since it creates a more stable plasma. The stability of the plasma is relevant, since a stable plasma is less likely to damage the structure.

The etch rate can be increased, by enhancing the removal of the passivation layer at the bottom of the trench. This can i.e. be done by increasing the bias voltage of the etching step. However this will increase the etch rate of the passivation layer of the sidewalls, which in turn will cause an increase in undercut and a bowing of the trench profile, according to Abdolvand and Ayazi, [31]. Chen et al. [28] reported that to increase the anisotropy (increase the vertical etch rate), without ruining the sidewall control the RF power can be increased, this would help remove the protective layer at the bottom of the trench.

3.2.3 Loading

Loading was observed between sample 11 and 15. Sample 11 was etched using the linear structure, created during the second optimization round, and 15 was etched using comb structure, used during the third optimization round. The difference in exposed silicon between these two structures is around 44 %. The difference in effective etch rates³ were 0.65 μm/min. for a difference in exposed silicon of about 44 %. This concur with the theory of a drop in etch rate, with an increase in exposed silicon, since the same concentration of fluorine radicals are etching more material.

A way to avoid this drop in etch rate, could be to simply scratch away some of the PMMA around the structure, this could easily reduce the exposed area of silicon and thereby increase loading reduced etch rate.

³The effective etch rate is the etch rate of the structure if one is only looking at the duration that the etching step is active. This does not take into account the fact that the passivation step might etch a small amount. The effective etch rate is calculated with a duration of the etching step of 14 seconds, this duration is used since it was the duration of the active etching cycle.

According to Juan and Pang, [32] a way to reduce the loading would be to decrease the pressure. This is done since the loading is an effect created by reactant depletion and at low pressures this has less effect.

3.2.4 Microtrench Formation and Etch Rate Uniformity

Microtrench formation

A formation of microtrenches at the bottom of the trench were observed on almost all samples using the comb structure, an example can be seen on sample 15 and 16, see figure 3.19 and 3.26. The microtrench width looks to be "constant", but since the trench width decreases, the microtrenches overlap and creates a hyperbolic triangle shaped bottom trench, see figure 3.21. The "constant" microtrench width can be seen in figure 3.22, 3.24, and 3.23, which show a narrowing of the microtrenches as the trench width decrease. The formation of microtrenches leads to some undesired effects, which will be discussed later. First the reason behind the microtrench formation will be discussed.

According to Westerheim et al. [33], the microtrench formation is created due to a higher fluorine concentration at the trench walls. This local increase in fluorine will lead to an increase in the local etch rate. The higher fluorine concentration is a result of reflected ions from the sidewalls.

Etch rate uniformity

The formation of these microtrenches are undesirable since it leads to a non-uniform etch rate. Sample 16 shows a difference in etch rate, which is dependant on the trench width. This can clearly be seen in figure 3.28. It is clear that the deeper trenches arises due to an etch rate non-uniformity. This etch rate non-uniformity is suspected to be a product of the formation of microtrenches, and not the usual ARDE, since the usual ARDE would decrease the etch rate in the narrow trenches and not increase it. The formation of microtrenches is more prominent than ARDE. Since the usual ARDE is less prominent, the etch rate is not limited by transport of the products from the trench, but limited by the transport to the trench.

According to Vyvoda et al. [29], the ion angular distribution (IAD) is dependant on the bias voltage. According of Westerheim et al. [33] the formation of microtrenches is very dependant on the IAD. To reduce the formation of microtrenches, the bias could be increased. In this reactor an increase in bias would have to come from a change in other parameters e.g. pressure. According to Jansen et al. [15] an increase in pressure (increase in bias and increase in plasma density) would result in a tighter IAD, which would decrease the formation of microtrenches.

3.2.5 Profile Control

The profile angle changes with duration of the passivation step. This can clearly be seen, by comparing sample 13 and 15, where the only difference is the duration of the passivation step. A change from 80 to 120 sec in passivation time show a change in profile angle of 6.5° , see figure 3.15 and 3.20. This shows that a change in duration of the passivation step will help control the profile angle.

The experiments related to profile control only investigates the connection between profile control and passivation duration. However other factors have an influence on the profile shape and angle. These factors include parameters like bias voltage, RF power, and pressure. During the second optimization round there is a noticeable difference in the amount of undercut and the profile angle, however no clear relation

between the individual parameters and the profile control, can be found due to the change in variables during the optimization of the process. The second optimization round was not meant as an investigation into the individual parameters influence on the profile angle, but was meant as an optimization of the entire Bosch process. According to Chen et al. [28] the profile control is in general, the combination of ion bombardment with the formation and preservation of the Teflon like film on the sidewalls. This fit perfectly with the experience gained during this project. According to this, settings that promote efficient removal of the protective films or promote the deposition of the protective film, have a high impact on the profile and the anisotropy of the trenches.

Bowing of the sidewall

The sidewall profile exhibits some bowing. This can clearly be seen in figure 3.28, where the very top of the sidewall is left hanging, insinuating that the profile exhibits some bowing. This bowing of the profile is undesired, since it diminishes the minimal width of a sidewall between two trenches. According to Abdolvand and Ayazi [31], the bowing is dependant on the bias voltage during the etching step. An increase in bias voltage will increase the number of scattered energetic ions from the bottom trench. This will in turn increase the amount of bowing, since the protective layer is attacked more.

The bowing of the sidewall profile can be reduced by reducing the bias of the etching step.

Profile control of different structures

Individual structures have individual "perfect" Bosch parameters. This can clearly be seen since the switch between sample 12 and sample 13 is only a change in structure (and number of cycles) but the sidewall is very different. The "perfect" window for the first linear structure, is not the "perfect" window for the comb structure, this is show by a clear difference in profile angle, see figure 3.12 and figure 3.15, where sample 12 exhibit a nice straight profile sample 13 exhibit a positive profile.

3.2.6 Scalloping, Undercut of the First Step and Other Sidewall Related Subjects

Scalloping

The characteristic scalloping of the sidewall can clearly be seen in figure 3.12. The scalloping is more prominent on sample 12, see figure 3.12, than on sample 16, see figure 3.27. This is due to a lower passivation to etching duration ratio. The scalloping arises due to the isotropic etching of fluorine radicals combined with the limited thickness of the passivation layer. The increase in scalloping formation from sample 16 to 12 can also be assigned to the loading effect, since the etch rate of sample 16 was lower than sample 12, which leads to an increase in the individual undercut of the cycle, hence more scalloping.

The scalloping of the sidewall has always been one of the drawbacks of the Bosch process, therefore a natural tendency towards the reduction of the scalloping is always present. Chabloz et al. [34] reduced the amount of scalloping from a peak-to-peak sidewall roughness of 105 nm to only 19 nm. This was done by modifying the etch/passivation balance as the etch progressed. This gave them a minimal sidewall roughness from the top to the bottom of the trenches, simultaneously with a highly anisotropic profile.

Undercut

Scalloping and undercut of the first step does not seem to be dependant on each other. Sample 12 and 17 both exhibit an undercut of the first step in the range of 315 nm. However the scalloping of sample 12 and 17 are very different, where sample 12 shows a more prominent scalloping than sample 17, see figure

3.13 and figure 3.32. The fact that the undercut is the same and that the scalloping is very different does again show, how the "perfect" parameters are structure dependant. The amount of undercut can not be reduced much further without some drastic changes and the sidewall is smooth and without scalloping. The amount of undercut is important since it defines the limit of how thin a wall between two trenches can be. In this case if we assume a straight profile with no bowing the wall between could no be thinner than 650 nm since a thinner wall would be destroyed.

Chabloz et al. [34] investigated a process of reducing the amount of undercut and the surface roughness. This was done by creating an equilibrium between the sputter removal rate of the passivation layer, the transportation of reactive etch species into the trenches, and the sputter desorption of the etch products out of the trenches. This results in a trench with almost no scalloping and a vertical profile. The equilibrium was maintained by chaining the process parameters, as the etch progressed. By varying the process parameters (mainly the bias and the duration of the passivation step) the undercut was decreased from 300 nm to only 100 nm.

Other Sidewall Related Subjects

The undercut of the first etching step was observed to be significantly larger than the others, see figure 3.12 and figure 3.27. The undercut can be explained with a missing sidewall protection of the first etching step.

The horizontal markings seen on figure 3.27 can be explained due to a more stable plasma. The software used to control the etch and passivation cycles was unable to handle more than 21 cycles. After the 21 cycles, the system had to be restarted. This restart lead to a more stable (more efficient) first etching step of each restart, which leads to the explanation of the horizontal markings, with a periodic separation.

Both the horizontal markings and the first etch are more prominent, than the rest of the sidewall scalloping. The explanation of this can be due to a more stable etching process. The first etch can also be explained by the fact that the sidewalls are missing, hence no sidewall passivation was present to protect the sidewall and this induced a deeper etch. This undercut of the first step can not be avoided, although it can be minimized, by decreasing the etching of the first step, hence the first step will not be as long and the passivation will take over and protect the sidewall. Regarding the horizontal markings these can be avoided by e.g. increasing the passivation time of the last step before the system is restarted, this will protect the sidewall from the more stable etching that comes from a restart.

3.2.7 Micrograss

In this section we focus on two kinds of micrograss, one kind is the micrograss that is outside the structure and the second kind is the one found inside the trenches, these will be referred to as external micrograss and internal micrograss, respectively. When talking about the micrograss in general the reference will simply be micrograss. This separation is done to differentiate between the two types of micrograss, since they are suspected to be the product of different mechanisms.

The main difference between the two formations are, as can be seen of figure 3.31 and figure 3.18. External micrograss is of different length and sizes, where internal micrograss is approximately the same size and length.

The external micrograss is suspected to be the product of micromasking sites, created by the sputtering and redeposition of the masking material, which in this case is Cr. This can be concluded due to the strong increase in the formation of external micrograss on sample 17, see figure 3.30. The only thing

changed between sample 16 and 17 was the thickness of the masking material. Another thing confirming the micromasking sites to be caused by the masking material, is the nonuniform height distribution, seen in figure 3.18. This is caused by the low sputtering rate of the masking material. This is verified by Oehrlein et al. [35], who investigated the formation of micrograss. The micrograss seen on top of the structure in figure 3.29 is also suspected to be external micrograss. All of this can be validated by XPS.

The cause behind the formation of the internal micrograss could not be determined. However it is still suspected to be caused by an other process than the sputtering and redeposition of the masking material. The cause could be investigated using XPS.

The internal micrograss is present on sample 17, see figure 3.31. As suggested by Dixit and Miao [25], the formation of micrograss will decrease as the trench width narrows. This can be seen in figure 3.30, where the density of the white spots decrease as the trench width decrease. According to observations, the formation of micrograss does not initiate in trenches with widths below $6 \mu\text{m}$. It was reported by Jo et al. [36] that at an $80 \mu\text{m}$ etch depth, the formation of micrograss occurred in open areas but not at the bottom of a $10 \mu\text{m}$ wide trench. The reason behind this is attributed to the difficulty of the redeposition of masking material, in a narrow deep trench. The fact that at an etch depth of $16.7 \mu\text{m}$ the micrograss can be found in narrower trenches is clear, since the decrease in depth, increases the probability of redeposition of masking material on the bottom trench.

The results show that at an AR above 2.8, micrograss can not be found. This can be defined as an AR threshold for the formation of micrograss. However the AR threshold for Jo et al. [36] is 8. This shows that the formation of micrograss can not be attributed as a single phenomena, but is dependant on more things, such as bias voltage, thickness of masking material, and RF power. However the AR threshold can be used as a guideline to the formation of micrograss if investigated more thoroughly.

3.2.8 Roughening Band

A roughening band can be seen on several of the samples. It can clearly be seen in figure 3.19. The roughening band is reduced from sample 15 to sample 16, this insinuates that the height of the roughening band is reduced, by increasing the thickness of the masking material.

According to Ayón et al. [16] and Bayt et al. [37], the size of the roughening band is determined by the process parameters (e.g. pressure, RF power) and the duration of the etching step. They assign the formation of the roughening band to the plasma damage done to the masking material and the subsequent transfer of this material to the sidewall. They use photoresist as a masking material and to minimize the roughening band a thin oxide layer was successfully placed on top of the structure, to reduce the damage towards the mask.

3.2.9 Bias Voltage

A series of experiments were conducted to investigate the influence of the other process parameters, such as flow rate and pressure, on the bias voltage. The results clearly show a drop in bias voltage, with an decrease in pressure. The flow rate does not affect the bias voltage very much, as can be seen in figure 3.7.

A high bias voltage during the passivation step will not only lead to a tighter IAD, it will also promote the etching domain, due to an enhanced energy of the impending ions. According to section 1.6, in the case of C_3F_8 , the bias needs to be below $\sim 130 \text{ V}$, for the polymerization domain to be dominant. If the

bias needs to be lower than ~ 130 V, then according to figure 3.6 the pressure need to be kept above ~ 175 mTorr (with the RF power kept at 250W). This will vary with a change in RF power, since the bias voltage also depends on the RF power.

Bias voltage has an effect on directionality of the impeding ions. This can be seen by the minimization of the undercut from sample 3 to sample 8, see figure 3.2 and figure 3.8. The difference between these samples can also be related to a difference in etch depth and etch rate, however the ratio between the etch depth and the undercut is still improved from 3.4 to 5 for sample 3 and 5 respectively. Abdolvand and Ayazi [31], investigated the influence of bias voltage on the trench profile. They discovered that the reduction of the bias voltage, from 42 V to 30 V, lead to an increase in silicon to mask selectivity. However the decrease in bias voltage also lead to the formation of sever sidewall striations. This is explained by the fact, that at a high bias voltage, the trajectory of the higher energetic ions is less likely to be disturbed, by the local electric fields, created by the charge build up on the sidewall passivation layer.

Polymer Deposition

The polymer formation depends very much on the bias voltage during the passivation step. For C_3F_8 , the boundary between the polymer enhanced domain and the etching domain, the bias voltage is very critical, since at a high bias voltage there is an induce switch, from the the polymer enhanced domain to the etching enhanced domain. This was observed during the first optimization round, but not fully understood until the second optimization round, where the bias voltage was lowered.

At an effect of 250 W, the bias voltage depends very highly on the pressure and not so much on the flow rate. This can clearly be seen in figure 3.6.

The deposition rate of C_3F_8 is low compared to the deposition rates of C_4F_6 and C_4F_8 in the article made by Wu et al. [12]. The deposition rates for C_4F_6 and C_4F_8 , at an RF power of 250 W, is 30 nm/min and 100 nm/min, respectively. The difference in disposition rates can be related to a lot of things, e.g. flow rate, bias voltage, F/C ratio, and pressure. The parameter with the highest influence is probably the bias voltage. In Wu et al. [12], the bias voltage can be controlled by the other independent RF power source, that is the main difference between DRIE reactors and normal RIE reactors. Based on this the deposition rate can be increased, by lowering the bias voltage, during the passivation step, even further. An increase in deposition rate could greatly reduce the production time.

3.2.10 Selectivity

A very important parameter is the relative silicon etch rate with respect to the masking material etch rate, i.e the etch selectivity. In this case, Cr was used to gain a high selectivity as opposed to the use of a photoresist, which has a lower selectivity. The selectivity of the Cr was over 1300:1. According to Williams et al. [38], the etch rate in Cr for a STS 320 PC RIE is below 1 nm/min, using the recipe: SF_6 Flow rate = 25 sccm, RF power = 100 W, pressure 20 mtorr. This indicates that the Bosch process helps increase the selectivity since the etch rate of the masking material is lower then the etch rate produced by Williams et al. [38].

According to Wu et al. [12] and Chen et al. [28], the etch rate of the masking material is dependant on the bias voltage, therefore to help increase the selectivity the bias voltage needs to be decreased. However if the bias voltage is increased so is the anisotropy, since the bias voltage controls the ion bombardment strength. The change in bias voltage is a trade-off between anisotropy and selectivity.

CR as Mask

Between the choices of a mask, Cr was selected to be used as a masking material. The other choices were photoresist, PMMA, Au, and Al. Since PMMA and the photoresist were to be used for different structures and they have a lower selectivity than the metal, they were unsuitable candidates for the masking material. Out of Cr, Al, and Au, Cr was selected on the basis that it was easier to lift-off, when using the sputter coater, than the other materials. Therefore a thicker layer of Cr could be deposited and the structure would still be cleared.

The sputtering of Cr, during the Bosch process, seemed to be thickness dependant. This is indicated by the drastically increase in sputtering, as the thickness got beyond a certain thickness. The sputtering is also dependent on the bias voltage and the RF power. Cr as a masking layer has shown a promising potential. It has however exhibited sputtering, but also a high selectivity.

In most other articles, photoresist is used as making layer, due to the complexity of adding a hard masking material. To protect the structure Chang et al. [39] used nickel. They observed an increase in grass formation, which was contributed to the sputtering of the masking material, due the addition of oxygen to the plasma. To counter the sputtering they suggested to use a more durable material, such as Cr or tungsten.

3.2.11 Choice of Passivation Gas and Gas Composition

C_3F_8 and CF_4 were available in the RIE setup, and of the two C_3F_8 was chosen as the passivation gas. This was done since it had the highest similarity to C_4F_8 , which is one of the most used gasses for the Bosch process. It was also chosen due to the higher F/C ratio which puts it at the interface between the polymerization and etching domains seen in figure 1.11. If CF_4 was chosen as the passivation gas, some hydrogen is needed in-order for the CF_4 to polymerize, instead of etching, according to figure 1.11.

Gas composition

The other gasses available were CHF_3 , O_2 , CF_4 , and He. This leads to the possibility that instead of using the flourcarbon based pulsed DRIE mode⁴, a switch could be made to use the oxygen based pulsed DRIE mode. Out of the two, according too Jansen et al. [15], the flourcarbon based process is more robust and show better results at room temperatures. The oxygen based is best at cryogenic conditions, where the conditions (temperatures at $-120^\circ C$) improves masking selectivity.

Sanaee et al. [40] used the oxygen based mixed DRIE mode⁵, which uses a combination of oxygen, hydrogen, and SF_6 during both the etching and passivation sub-sequence. At room temperature an aspect ratios as high as 100, with a mask undercut of only 30 nm was achieved.

In order to achieve a HAR structure, Abdolvand and Ayazi [31] added two new steps to the Bosch process. The first step in between the passivation step and the etching step, as a depassivation step, and the second step after the etching. It was practically done by using Argon in the depassivation plasma pulse to remove the passivation layer at the bottom of the trench. The second step after the etching step was a short oxygen-clean pulse to improve trench-profile uniformity, by efficiently removing polymer residues from the structure. So by changing the gas, a higher aspect ratio was achieved.

⁴The pulsed mode is the same as the normal Bosch process.

⁵The mixed-mode is a mode where the different gasses are all present during all the steps, but the flow rate of the individual gasses are changed.

Stability of the RIE Chamber

In an attempt to keep the process reproducible and the etch rate uniformity at a stable level, just as Jansen et al. [15], the reactor chamber was cleaned after approximately 6-8 hr use. This was done by exposing the chamber to an oxygen plasma at 50 W for approximately 1 hour. The oxygen plasma would remove the polymer residue, still sticking to the reactor sidewalls.

The attempt in stabilizing the RIE reactor was done without seasoning the chamber afterwards. A seasoning of the chamber is, according to McColman [41] and Jansen et al. [15], very important to the repeatability of the Bosch process. They showed that the etch rate rises and that the etch rate uniformity drops, with respect to seasoning time. McColman [41] observed an increase in etch rate, from $2.4 \mu\text{m}/\text{min}$ to $3 \mu\text{m}/\text{min}$, after 10 hours of seasoning.

In this project the seasoning of the reactor chamber was not carried out and could include some instabilities regarding the reproducibility of the experiments.

3.2.12 Aspect Ratio

Brincker and Karlsen [1], created the theoretical lens design with an AR off 40. This AR was based upon the structure created by Brückner et al. [42]. The fabricated structure was a structure of pillars, with spacings between the pillars of $12.5 \mu\text{m}$ and a depth of $500 \mu\text{m}$. The masking material was, as in this project, Cr, with a thickness of 500 nm.

Sample 16 had an AR of 22, and lens 1 had a presumed AR of 10. The limiting factor for a HAR structure is, in this case, the selectivity and the thickness of the Cr. Sample 16 is a good example of a masking material layer that is too thin. When it is too thin, the material is etched through and the structure underneath is deteriorated, as can be seen in figure 3.28. So the masking material thickness sets an upper limit to the maximum achievable AR.

To achieve a HAR structure, the selectivity needs to be lowered, and a solution has to be found regarding the formation of micrograss, since an increase in masking material thickness increases the formation of micrograss, as can be seen in figure 3.30.

3.2.13 Summary

Future work would require some more optimizing, regarding the Bosch process. This involves dealing with: the formation of micrograss, increasing the selectivity, and the bowing of the sidewalls. These are probably the most important things, then there is the secondary problems which involves, finding a solution to the high production time and finding a solution to the formation of microtrenches.

The most important thing to investigate is the increase in selectivity and afterwards the investigation of the bowing of the sidewalls, would be a natural step.

Apart from all this there is the problem regarding the fabrication of the mask for the full size lens structure. This problem could be solved by stitching write fields together, to write the entire structure in one take. If the structure is changed then the Bosch process needs to be optimized to the new structure.

The optimal process parameters for the three structures fabricated in this project, can be found in table 2.1 and 2.2. The "perfect" window for the three structures are those of sample 12, sample 16 and lens 1.

Conclusion 4

Since the THz regime is of such great interest and has so many interesting applications, it is important to have the tools to use it. This is where the investigation into the fabrication of different lens designs comes into play. They acts as the tools to manipulate the THz radiation.

The aim of this report was to fabricate a GRIN lens based on the design proposed by Brincker and Karlsen [1]. To do this a basic understanding revolving the fabrication of HAR structures was first needed. To fabricate the HAR structures the Bosch process was investigated and found suitable.

This report investigated the fabrication of HAR structures using a STS 320 PC RIE. A systematic optimization of the Bosch process, utilizing SF₆ as an etching gas and C₃F₈ as a passivation gas, was presented, in order to fabricate HAR structures with vertical sidewalls. The Bosch process was optimized and structures with vertical sidewalls and an AR of 22, was successfully fabricated. The Bosch process showed high stability and the ability to control the angle of the sidewalls. The sidewall scalloping of the Bosch process was observed, but the scalloping of the sidewalls was less on the smaller structures than on the larger.

The overall etch rate of the system was low, compared to the etch rate of previous experiments, and therefore future investigations into an increase in etch rate could lower the fabrication time significantly.

The formation of microtrenches were observed and investigated. The formation of microtrenches gave a non-uniform etch rate in the 2 μm wide trenches, compared to that of the wider trenches. It was concluded that the microtrenches was a result of sidewall effects. This non-uniform etch rate is undesired since it can lead to some unwanted effects regarding the GRIN lens.

Chromium as a masking material offers a high selectivity and minimum lift-off related problems. However at high bias voltages, chromium showed an increase regarding the redeposition and creation of micrograss, also called black silicon, which is an undesired effect.

It can be concluded that some improvements have to be made to achieve structures with an AR above 22.

Bibliography

- [1] Mads Brincker, Peter Karlsen, “Compact thz photo-conductive antenna with an integrated microstructured substrate lens,” tech. rep., Aalborg University, 2014.
- [2] A. Rostami, H. Rasooli, and H. Baghban, *Terahertz Technology: Fundamentals and Applications*. Lecture Notes in Electrical Engineering, Springer, 2010.
- [3] M. C. Kemp, “Explosives detection by terahertz spectroscopy: a bridge too far?,” *Terahertz Science and Technology, IEEE Transactions on*, vol. 1, no. 1, pp. 282–292, 2011.
- [4] M. Van Exter, C. Van Exter, D. Fattinger, and Grischkowsky, “High-brightness terahertz beams characterized with an ultrafast detector,” vol. 55, pp. 337–, 1989.
- [5] P. U. Jepsen and S. Keiding, “Radiation patterns from lens-coupled terahertz antennas,” *Optics letters*, vol. 20, no. 8, pp. 807–809, 1995.
- [6] E. Hecht, *Optics*. Pearson education, Addison-Wesley, 2002.
- [7] S. C. Saha, C. Li, Y. Ma, J. P. Grant, and D. Cumming, “Fabrication of multilevel silicon diffractive lens at terahertz frequency,” *Terahertz Science and Technology, IEEE Transactions on*, vol. 3, no. 4, pp. 479–485, 2013.
- [8] S.-G. Park, K. Lee, D. Han, J. Ahn, and K.-H. Jeong, “Subwavelength silicon through-hole arrays as an all-dielectric broadband terahertz gradient index metamaterial,” *Applied Physics Letters*, vol. 105, no. 9, p. 091101, 2014.
- [9] G. Savini, P. A. Ade, and J. Zhang, “A new artificial material approach for flat thz frequency lenses,” *Optics express*, vol. 20, no. 23, pp. 25766–25773, 2012.
- [10] B. Bhushan, *Springer Handbook of Nanotechnology*. Gale virtual reference library, Springer, 2007.
- [11] E. Bassous, “Fabrication of novel three-dimensional microstructures by the anisotropic etching of (100) and (110) silicon,” *IEEE Trans. Electron Devices*, vol. 25, no. 10, pp. 1178–1185, 1978.
- [12] B. Wu, A. Kumar, and S. Pamarthy, “High aspect ratio silicon etch: A review,” *Journal of applied physics*, vol. 108, no. 5, p. 051101, 2010.
- [13] A. P. Nayak, M. S. Islam, and V. Logeeswaran, “Wet etching,” *Encyclopedia of Nanotechnology*, pp. 2829–2830, 2012.

- [14] V. Lindroos, S. Franssila, M. Tilli, M. Paulasto-Krockel, A. Lehto, T. Motooka, and V. Airaksinen, *Handbook of Silicon Based MEMS Materials and Technologies*. Micro and Nano Technologies, Elsevier Science, 2009.
- [15] H. Jansen, M. De Boer, S. Unnikrishnan, M. Louwerse, and M. Elwenspoek, “Black silicon method x: a review on high speed and selective plasma etching of silicon with profile control: an in-depth comparison between bosch and cryostat drie processes as a roadmap to next generation equipment,” *Journal of Micromechanics and Microengineering*, vol. 19, no. 3, p. 033001, 2009.
- [16] A. A. Ayón, R. Braff, C.-C. Lin, H. H. Sawin, and M. A. Schmidt, “Characterization of a time multiplexed inductively coupled plasma etcher,” *Journal of the Electrochemical Society*, vol. 146, no. 1, pp. 339–349, 1999.
- [17] M. Shearn, X. Sun, M. D. Henry, A. Yariv, and A. Scherer, *Advanced plasma processing: etching, deposition, and wafer bonding techniques for semiconductor applications*. InTech, 2010.
- [18] P. Verdonck, “Plasma etching,” in *Oficina de Microfabricação: Projeto e Construção de CIs MOS* (J. Swart, I. Doi, and J. Diniz, eds.), Campinas, Universidade Estadual de Campinas, 2006.
- [19] H. Jansen, H. Gardeniers, M. de Boer, M. Elwenspoek, and J. Fluitman, “A survey on the reactive ion etching of silicon in microtechnology,” *Journal of micromechanics and microengineering*, vol. 6, no. 1, p. 14, 1996.
- [20] M. Madou, *Manufacturing Techniques for Microfabrication and Nanotechnology*. Fundamentals of Microfabrication and Nanotechnology, Taylor & Francis, 2011.
- [21] E. Iannone, *Labs on Chip: Principles, Design and Technology*. Devices, Circuits, and Systems, Taylor & Francis, 2014.
- [22] V. M. Donnelly and A. Kornblit, “Plasma etching: Yesterday, today, and tomorrow,” *Journal of Vacuum Science & Technology A*, vol. 31, no. 5, p. 050825, 2013.
- [23] Center of Micronanotechnology CMI, *Manual for AMS 200 SE (Silicon Etcher)*. Ecole polytechnique federale de Lausanne, URL: <https://cmi.epfl.ch/etch/AMS200.php>, 2010. Downloaded: 16-04-2015.
- [24] W. Juan and S. Pang, “High-aspect-ratio si etching for microsensor fabrication,” *Journal of Vacuum Science & Technology A*, vol. 13, no. 3, pp. 834–838, 1995.
- [25] P. Dixit and J. Miao, “Effect of sf6 flow rate on the etched surface profile and bottom grass formation in deep reactive ion etching process,” in *Journal of Physics: Conference Series*, vol. 34, p. 577, IOP Publishing, 2006.
- [26] Anders Tang, Sofia Ferreira, “Fabrication and characterization of silicon nanowire field-effect transistors,” tech. rep., Aalborg University, URL: <http://projekter.aau.dk/projekter/files/172982950/report.pdf>, 2013. Downloaded: 21-04-2015.
- [27] M. Fischer, M. Stubenrauch, T. Kups, H. Romanus, F. Morales, G. Ecke, M. Hoffmann, C. Knedlik, O. Ambacher, and J. Pezoldt, “Self organization and properties of black silicon,” 2006.

- [28] K.-S. Chen, A. Ayón, X. Zhang, S. M. Spearing, *et al.*, “Effect of process parameters on the surface morphology and mechanical performance of silicon structures after deep reactive ion etching (drie),” *Microelectromechanical Systems, Journal of*, vol. 11, no. 3, pp. 264–275, 2002.
- [29] M. Vyvoda, H. Lee, M. Malyshev, F. Klemens, M. Cerullo, V. Donnelly, D. Graves, A. Kornblit, and J. Lee, “Effects of plasma conditions on the shapes of features etched in cl₂ and hbr plasmas. i. bulk crystalline silicon etching,” *Journal of Vacuum Science & Technology A*, vol. 16, no. 6, pp. 3247–3258, 1998.
- [30] A. Ayón, R. Braff, R. Bayt, H. Sawin, and M. Schmidt, “Influence of coil power on the etching characteristics in a high density plasma etcher,” *Journal of the electrochemical Society*, vol. 146, no. 7, pp. 2730–2736, 1999.
- [31] R. Abdolvand and F. Ayazi, “An advanced reactive ion etching process for very high aspect-ratio sub-micron wide trenches in silicon,” *Sensors and Actuators A: Physical*, vol. 144, no. 1, pp. 109–116, 2008.
- [32] W. Juan and S. Pang, “High-aspect-ratio si etching for microsensor fabrication,” *Journal of Vacuum Science & Technology A*, vol. 13, no. 3, pp. 834–838, 1995.
- [33] A. Westerheim, A. Labun, J. Dubash, J. Arnold, H. Sawin, and V. Yu-Wang, “Substrate bias effects in high-aspect-ratio sio₂ contact etching using an inductively coupled plasma reactor,” *Journal of Vacuum Science & Technology A*, vol. 13, no. 3, pp. 853–858, 1995.
- [34] M. Chabloz, Y. Sakai, T. Matsuura, and K. Tsutsumi, “Improvement of sidewall roughness in deep silicon etching,” *Microsystem Technologies*, vol. 6, no. 3, pp. 86–89, 2000.
- [35] G. Oehrlein, J. Rembetski, and E. Payne, “Study of sidewall passivation and microscopic silicon roughness phenomena in chlorine-based reactive ion etching of silicon trenches,” *Journal of Vacuum Science & Technology B*, vol. 8, no. 6, pp. 1199–1211, 1990.
- [36] S.-B. Jo, M.-W. Lee, S.-G. Lee, E.-H. Lee, S.-G. Park, *et al.*, “Characterization of a modified bosch-type process for silicon mold fabrication,” *Journal of Vacuum Science & Technology A*, vol. 23, no. 4, pp. 905–910, 2005.
- [37] R. L. Bayt, A. Ayon, and K. Breuer, “A performance evaluation of mems-based micronozzles,” *AIAA paper*, no. 97-3169, 1997.
- [38] K. R. Williams, K. Gupta, and M. Wasilik, “Etch rates for micromachining processing-part ii,” *Microelectromechanical Systems, Journal of*, vol. 12, no. 6, pp. 761–778, 2003.
- [39] Y.-F. Chang, Q.-R. Chou, J.-Y. Lin, and C.-H. Lee, “Fabrication of high-aspect-ratio silicon nanopillar arrays with the conventional reactive ion etching technique,” *Applied Physics A*, vol. 86, no. 2, pp. 193–196, 2007.
- [40] Z. Sanaee, M. Poudineh, M. Abdolahad, and S. Mohajerzadeh, “High aspect ratio micro-and nano-machining of silicon using time-multiplexed reactive ion etching,” *Journal of Micromechanics and Microengineering*, vol. 21, no. 12, p. 125012, 2011.

- [41] Shane McColman, "Advanced bosch processing on the oxford plasmalab icprie," tech. rep., University of Alberta, URL: http://www.nanofab.ualberta.ca/wp-content/uploads/2009/05/bosch_advanced.pdf, 2009. Downloaded: 20-07-2015.
- [42] C. Brückner, T. Käsebier, B. Pradarutti, S. Riehemann, G. Notni, E.-B. Kley, and A. Tünnermann, "Broadband antireflective structures applied to high resistive float zone silicon in the thz spectral range," *Optics express*, vol. 17, no. 5, pp. 3063–3077, 2009.

Appendix A

| Name | Ramp Time (s) | Deposition time (s) | RF Power (W) | Thickness (nm) |
|------|---------------|---------------------|--------------|----------------|
| Cr1 | 7 | 9 | 400 | 12 |
| Cr2 | 7 | 15 | 400 | 20 |
| Cr3 | 7 | 11 | 400 | 15 |
| Cr4 | 7 | 25 | 400 | 33 |
| Cr5 | 7 | 50 | 400 | 67 |

Table A.1: Table showing the individual parameters used during the sputtering of Cr on the samples.